NIST-GCR-96-695

DEVELOPMENT OF AN ECONOMICAL VIDEO BASED FIRE DETECTION AND LOCATION SYSTEM

O.A. Plumb and R.F. Richards

Department of Mechanical and
Materials Engineering
Washington State University
Pullman, WA 99164-2920

July 1996

U.S. Department of Commerce
Michael Kantor, *Secretary*
Technology Administration
Mary L. Good, *Under Secretary for Technology*
National Institute of Standards and Technology
Arati Prabhakar, *Director*

Notice

This report was prepared for the Building and Fire Research Laboratory of the National Institute of Standards and Technology under grant number 60NANB2D1290. The statement and conclusions contained in this report are those of the authors and do not necessarily reflect the views of the National Institute of Standards and Technology or the Building and Fire Research Laboratory.

DEVELOPMENT OF AN ECONOMICAL VIDEO BASED FIRE DETECTION AND LOCATION SYSTEM

O.A. Plumb and R.F. Richards
Department of Mechanical and Materials Engineering
Washington State University
Pullman, WA 99164-2920

Contents

Abstract

A method of detecting, locating, and sizing accidental fires based on the solution of an inverse heat transfer problem is described and a prototype video fire detection system employing that method is presented. The inverse heat transfer problem to be solved is that of the convective heating of a compartment ceiling by the hot plume of combustion gases rising from an accidental fire. An inverse problem solution algorithm capable of determining the location and heat release rate of the fire employing transient temperatures at the ceiling of the compartment as data is developed. A prototype system based on the use of a video camera to monitor an array of temperature-sensitive, color-changing sensors and capable of supplying the transient temperature data needed by the inverse problem solution algorithm is described. The limits on the accuracy of the inverse problem solution algorithm are demonstrated by exercising the algorithm, on transient temperature data from computer simulated compartment fires. The performance of the prototype video fire detection system is demonstrated by employing it to determine the location and heat release rate of a small flame source in a lab scale test enclosure.

1 Introduction

In this report we present the results of work directed toward the development of a working prototype of a system that can automatically detect, locate, and size an accidental fire. The fire detection system uses a video camera to gather temperature data from an array of temperature-sensitive, color-changing sensors distributed around a compartment, and a personal computer based inverse problem solution algorithm to determine the fire's location and heat release rate using the gathered temperature data. Such a system offers great promise for use in industrial facilities such as warehouses and factory floors which combine significant fire risks with minimal human monitoring for extended periods. When accidental fires do occur in these kinds of settings, the time the fire burns undetected plays a crucial role in the destructiveness of the fire. As a result there is a critical need for an economical means to automatically monitor work spaces and quickly determine the presence of a fire and assess the threat to life and property.

Fire protection systems now in service, such as fusible link sprinklers, can automatically detect and act to suppress accidental fires without human intervention. However, these systems have only a rudimentary ability to determine the location and size of the fire. Such systems lack the intelligence to direct suppression measures (automatic or human) so as to maximize fire-fighting effectiveness and minimize collateral damage from water or chemical suppressants. Fire protection systems now being developed are remedying this shortcoming by taking advantage of recent advances in sensor and microprocessor technology. These new systems incorporate the intelligence to locate a fire, determine its threat, and precisely direct suppression. For example Ref. [1] describes a machine vision system that uses a video camera, along with infrared and ultraviolet sensors, to locate a fire and determine its physical dimensions. Reference [2] reports on progress toward the development of an artificial nose which employs a neural net to discriminate odors and identify the fuel source of a fire. Reference [3] discusses the use of fiber optic sensors to locate fires by monitoring local temperatures around a compartment .

Inverse problem solution methods represent a new route toward intelligent fire detection systems. These methods constitute suite of powerful techniques that can be

applied to the problem of fire detection. The theory of inverse heat transfer problems, is quite well developed. For example, the recovery of the location and/or heat release rates of heat sources in thermally conducting solids [4], in radiating gases [5], and in convective flow situations [6] given a limited number of discrete temperature or heat flux measurements has been demonstrated by various workers .

The heat transfer problem of interest in the problem of fire detection is the convective heating of a compartment ceiling by the buoyant plume and resulting ceiling jet of hot combustion gases originating from an accidental fire. Solution of the inverse heat transfer problem involves comparing transient temperature information gathered by sensors situated at discrete locations on the ceiling to predictions of those temperatures by a numerical fire model. Minimizing the residuals between measured and predicted temperatures gives the most probable location and heat release rate of the fire which generated the plume and ceiling jet.

This report is broken down into two parts. In the first part, the method of solution of the inverse fire detection problem, the inverse problem solution algorithm, is developed. Details of the inverse problem solution algorithm, which is based on the compartment fire zone model LAVENT, are given.

The limits on the performance of a fire detection system based on the inverse problem solution are evaluated by simulating the operation of the system using computer synthesized fire data. The accuracy of the inverse problem solution based detection system in determining the locations and the heat release rates of the simulated fires is quantified on a statistical basis. The effects of random measurement error and systematic model error on the accuracy of the inverse problem solution are quantified. The speed of fire detection is determined. The use of computer simulated fire data in the evaluation of the inverse problem solution algorithm, is validated by comparing the results of the evaluation with a second evaluation based on fire data interpolated from published measurements taken in large-scale experimental compartment fire burns.

In the second part of the report the implementation of the inverse problem solution algorithm in a working prototype of a fire detection, location and sizing system is reported.

The design and operation of the prototype version of the inverse problem solution based intelligent fire detection system is described. The system uses an inexpensive black and white video camera to monitor temperature-sensitive, color-changing sensors distributed around a compartment. . In the event of a fire, the sensors change color in response to convective heating from the fire plume. The video camera detects the change in color of the activated sensors and relays the time of the color change along with the location of the activated sensor to a personal computer. The personal computer determines the location and heat release rate of the fire by implementing the inverse problem solution algorithm, with the times of activation (color change) of the sensors used as data for the algorithm.

An evaluation of the prototype video fire detection system is presented and the results of the evaluation discussed. The evaluation focuses on three aspects of the fire detection system's operation. First, the ability of the video system to monitor the passive sensors and determine the activation of the temperature-sensitive, color changing sensors is verified. Second, the accuracy of the prototype system in locating a flame source placed at random locations in a laboratory-scale test enclosure and in determining the heat release rate of the flame source is reported. Third, the ability of the prototype system to detect the presence of smoke and determine the optical thickness of the smoke is evaluated.

2 Theory: Fire Detection by Inverse Problem Solution

The inverse fire detection problem is illustrated in Fig. 1. If a fire is accidentally ignited in a compartment, a buoyant plume of hot combustion gases will be generated. The buoyant plume will rise to the ceiling of the compartment and upon reaching the ceiling turn and flow radially outward as a ceiling jet. As the ceiling jet spreads radially, the ceiling will be convectively heated. Temperature sensors, T1 through T6, placed at discrete locations on or near the ceiling will also be heated by the ceiling jet. If the temperature sensors are such that they are activated at a temperature between the ceiling jet temperature and ambient temperature, then those sensors will be activated one by one as the ceiling jet spreads radially outward. The inverse problem to be solved is to determine the location, (x,y), and

heat release rate, Q, of the fire, given the times at which individual temperature sensors reach their activation temperature.

2.1 Solution of the Inverse Fire Detection Problem

The problem of locating a fire and determining its growth rate can be formally posed as an inverse problem in which the times of activation, t_i, of n ceiling mounted sensors (where $i = 1, n$) are used as data to find two unknown parameters determining the fire location: x, y, and one unknown parameter determining the fire growth rate: α. The problem is thus one of parameter estimation. The location of the fire is described by the Cartesian coordinates, (x,y), where the fire is assumed to lie in the plane of the compartment floor. The fire growth rate is determined by the parameter α, which follows from the functional form of the fire heat release rate assumed in the present work:

$$Q = \alpha_t^2 \qquad (1)$$

The quadratic form is chosen following Heskestad's recommendation in Ref. [7] for the initial stages of fire growth. Here Q is the fire's convective heat release rate in W, and t is the elapsed time from the ignition of the fire in seconds. The parameter to be found, α, is seen to have units of Ws^{-2}.

Solution of the inverse problem requires two steps: first prediction of the transient temperature field in the compartment using a numerical fire model, and second minimization of the residuals between measured and predicted temperatures to determine the most probable location and heat release rate for the fire. The first step, prediction of the temperature field given the heat source, is commonly referred to as solution of the forward problem. The second step, comparison of transient temperature data gathered by sensors to predictions of those temperatures by the numerical fire model to obtain location and heat release rate information about the fire, completes solution of the inverse problem. Together these two steps are implemented on a personal computer as an inverse problem solution algorithm.

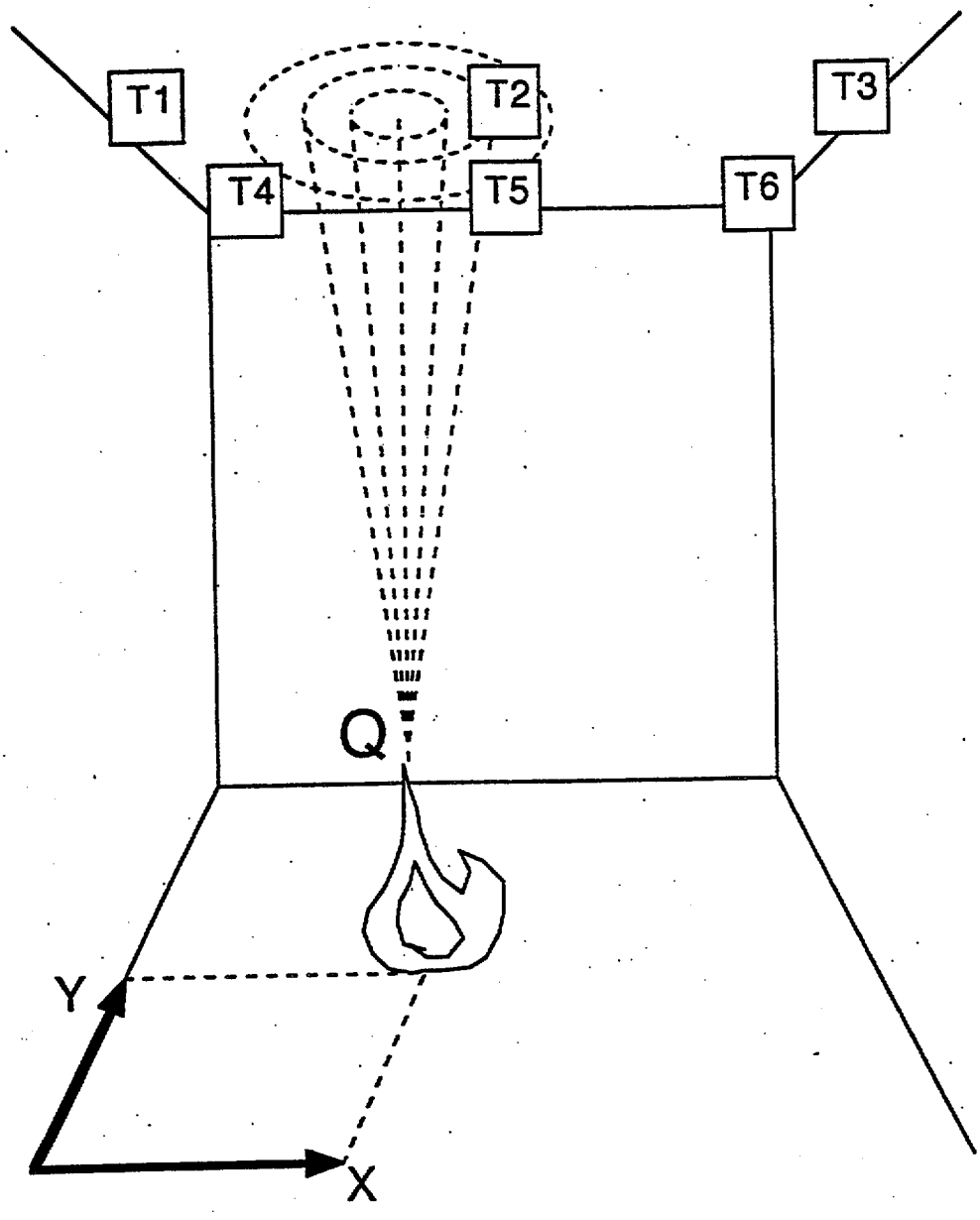

Figure 1. The inverse fire detection problem.

In the present study, the first step of the inverse problem solution algorithm, the solution of the forward problem is found using the compartment fire model LAVENT [8]. LAVENT, a two-zone fire model employing semi-empirical models of the buoyant plume and ceiling jet, is able to compute convective heat fluxes from a fire to the ceiling of a compartment. LAVENT assumes that interactions between the plume and side wall are negligible, and that the compartment air is quiescent so that both the buoyant plume and ceiling jet remain axially symmetric about a vertical line drawn through the fire.

Forward problem solutions are found for a set of many fire scenarios. Each fire scenario consists of a fire with a given location and growth rate, (x,y,α), in the relevant compartment geometry. The zone fire model LAVENT, is employed to predict the transient temperature field across the compartment ceiling for each fire scenario (x,y,α) in the set. Using the transient temperature solution for each scenario from LAVENT, the times at which each sensor will be activated can be determined, given both the locations of the temperature-sensitive sensors and their activation temperature. The predicted activation time for each sensor is then defined to be the elapsed time from the time the first sensor changes color:

$$t_{a,i} = t_i - t_1. \qquad (2)$$

In this way, activation times for a complete set of fire scenarios, that is, for all possible fire locations and growth rates, can be generated. This collection of predicted activation times covering all possible fire scenarios constitutes the database of forward problem solutions used for the inverse problem solution.

In the present study a complete set of fire scenarios consists of eight discrete fire growth rates in the range $0.001 < \alpha < 0.06$ kW/s^2, and 400 fire locations situated on a square grid at increments of $0.05d$ (where d is the distance between sensors) in x and y. Due to symmetry only 66 of the 400 fire locations are unique. Therefore, a complete set of forward problem solutions involves a database of only 528 fire scenarios. Forward problem solutions can be pre-calculated and stored in computer memory. The solutions are stored in

the form of the locations and activation times of the first five sensors to be set off by the fire: $(x_i, y_i, t_{a,i})$ where $i = 1$ to 5.

Given a complete set of forward solutions, the second step of the inverse problem solution algorithm can be implemented: the comparison of measured and predicted transient temperature data. The data required for the inverse problem solution are the times at which individual sensors are activated as a result of the plume of hot gases rising from the fire. Measured activation times for the first five sensors activated ($i = 1$ to 5) in a given fire scenario are required, where the measured activation time for each sensor is taken as the elapsed time from the time the first sensor changes color:

$$\hat{t}_{a,i} = \hat{t}_i - \hat{t}_1 \tag{3}$$

The inversion algorithm proceeds by subtracting measured activation times from predicted activation times and then summing the squares of the differences:

$$S = \sum_{i=1}^{n} \left(t_{a,i} - \hat{t}_{a,i} \right)^2 \tag{4}$$

The solution to the inverse problem is taken to be the values of the parameters x, y, and α for the fire scenario which minimizes the sum of squares, S, over the complete set of fire scenarios. The minimum of S is found through the technique of exhaustive search. The sum of squares, S is calculated for each of the 528 fire scenarios in a complete set and the minimum value found by comparing the values of S determined for each scenario. In those cases where two or more fire scenarios produce equal minima of S, the average of the respective values of x, y, and α are taken as the solution.

2.2 Evaluation of the Inverse Problem Solution Algorithm

Two tests were undertaken to evaluate the inverse problem solution algorithm. First, the accuracy of the algorithm was evaluated using computer simulated fire data. Second, the use of the computer simulated data to test the algorithm was validated using fire data interpolated from measurements taken in full scale experimental burns.

The accuracy of the inverse problem solution algorithm in locating and sizing accidental fires largely depends on the algorithm's sensitivity to two kinds of error: random errors in the transient temperature measurements, and the systematic errors in the forward problem solution. Random errors in sensor activation times must be expected regardless of the type of sensor used to gathered the data required by the inversion algorithm. Likewise, any fire model used to produce the forward problem solution will have associated with it some limitations, assumptions, or simplifications which will result in systematic errors in that solution.

To evaluate the performance of the inverse problem solution algorithm, the algorithm was exercised on test cases consisting of computer simulated fire data. Quantification of the effect of the errors described above, was accomplished by corrupting the original simulated fire data by adding to the data random and systematic errors of known magnitude. The fire location and heat release rate predicted by the inverse problem solution algorithm using the corrupted fire data (data with errors) was then compared to the fire location and heat release rate which was assumed to produce the original uncorrupted fire data.

The usefulness of an evaluation of the inverse problem solution algorithm based on computer simulated compartment fire data, such as that just described, depends upon the degree to which the computer simulated fire data resembles real data produced by real fires. For this reason a second evaluation of the inverse problem solution algorithm was run using data measured in large-scale experimental compartment fire burns. In order to determine sensor activation times for sensors at locations other than those instrumented in the original experiments, a system of interpolation was used. The system of interpolation produced temperature versus time data for any location in a compartment, using data measured at a few discrete location in the compartment.

2.2.1 Computer Simulation of Compartment Fire Data

The first evaluation of the inverse problem solution algorithm began by simulating a compartment fire with a given location and growth rate (x,y,α) using the zone fire model LAVENT. Sensor activation times were determined given the sensor location and the

transient temperature field at the compartment ceiling calculated by LAVENT for a fire with the assumed location and growth rate.

All simulations were run assuming a compartment similar to the warehouse used for the large-scale test burns reported in Ref. [9]. The compartment was taken to be 3 meters high, 20 wide, and 20 meters deep, with a smooth, insulated ceiling. The compartment was assumed to be completely enclosed, without sources of ventilation. The ambient temperature in the compartment was taken to be constant at T_{amb} = 300 K. The temperature sensors for the detection system were assumed to be distributed on a square grid, spaced three meters apart. The activation temperature for all sensors was selected to be T_a= 311 K. The sensors were assumed to hang in the hottest part of the ceiling jet, between 0 and 10 cm from the ceiling. The sensors were taken to have negligibly small thermal mass, so that their time response would be essentially instantaneous.

To enable the quantification of the effects of uncertainty that would inevitably arise in a real fire detection system, errors were added to the sensor activation times determined from the LAVENT simulated fire data. In this way corrupted data were produced which more closely resembled sensor activation times that would be measured during a real fire, than the original LAVENT simulated data.

Two types of error were added to the LAVENT simulated data. To account for limitations or inaccuracy inherent in the fire model used to produce the forward solution, a systematic error was added to the simulated sensor activation times. The systematic model error was assumed to be composed of a constant bias and a component which grew linearly in elapsed time. To account for uncertainty in the sensor activation time measurements, a random error was also added to the LAVENT simulated activation times. The random measurement errors, were assumed to follow a Gaussian distribution with a mean value of zero. Adding the systematic and random errors to the original LAVENT simulation activation time for the i^{th} sensor, $t_{LAV,i}$, the corrupted activation time of the i^{th} sensor, $t_{a,i}$ could be calculated:

$$\hat{t}_{a,i} = \hat{t}_{LAV,i} + (a + b\hat{t}_{LAV,i}) + G(\sigma) \qquad (5)$$

where a and b are constants characterizing systematic error, and $G(\sigma)$ is a random number chosen from a normal distribution with standard deviation σ. Note that the parameter a has units of seconds and represents a constant time bias. The parameter b, which has a dimensionless value between zero and unity, represents an error which is always a constant fraction of the elapsed time.

2.2.2 Interpolation of Measured Compartment Fire Data

To validate the use of simulated fire data in the evaluation of the inverse problem solution algorithm and to verify that such an evaluation yields realistic results, a parallel evaluation based on experimental measurements was undertaken. Measurements made during large scale test burns of wood crib fires at the Factory Mutual Research Center by Heskestad and Delichatsios and reported in Ref. [9] provided a set of realistic fire data. In that paper, measurements of ceiling jet temperatures were given versus time and radius from the fires, for eight different fires. Unfortunately, the ceiling jet temperatures reported in Ref. [9] were given at only six radial locations. As a result, a means to 'interpolate' transient temperature data, at radial distances between those distances for which Ref. [9] reported measurements, was employed.

The interpolation of transient temperature data from the measurements was accomplished by fitting the measurements to a general form of the correlation given as Eq. (1) in Ref. [9]

$$t(r) = c_1\left(T(r) - T_{amb}\right)^{3/4} + c_2\left(T(r) - T_{amb}\right)^{3/4}(r/h) + c_3(r/h) + c_4 \qquad (6)$$

where $T(r)$ is the ceiling jet temperature at radius r, $t(r)$ is time elapsed from the start of the fire, h is the ceiling height, and c_1, c_2, c_3, and c_4 are constants. In the present work, elapsed time is chosen as the dependent variable and temperature as the independent variable, because the inversion algorithm uses as data the times at which sensors at various radii from the fire plume reach their activation temperature. Once the correlation, Eq. (6) was fitted to the measurements from Ref. [9] using least squares, residuals for the data with respect to the correlation were calculated. The residuals were tabulated by counting the number of residuals that fell into bins between the lowest and highest values of the residuals (-12 s < r

<10 s), where each bin was one second wide. In this way a probability density function for the residuals was constructed. The pdf determined was found to be approximated by a Gaussian distribution with a mean value of 0 s and standard deviation of 4.7 s.

Using Eq. (6) with the appropriate constants c_1, c_2, c_3, and c_4, and the pdf found for the residuals it was possible to generate new time versus temperature data. The new data was generated by using the correlation to calculate a time, $t(r)$, at which a given temperature, $T(r)$, would be reached at any radial position, r. Values randomly chosen from the residual pdf were then added to the time, $t(r)$, resulting from the correlation. Time versus temperature data generated in this way would be indistinguishable from the original measurements reported in Ref. [9].

2.2.3 Evaluation of the Inverse Problem Solution Algorithm: Computer Simulated Fire Data

A test of the inverse problem solution algorithm was run by randomly selecting a fire location, (x_{sim}, y_{sim}), in the range $0 < x_{sim} < d$, $0 < y_{sim} < d$, and a fire growth rate, α_{sim}, in the range $0.001 < \alpha_{sim} < 0.06$ kWs^{-2}. LAVENT was run to simulate the transient temperature history at the compartment ceiling for the given fire location and growth rate. The LAVENT generated transient temperatures were then used to determine sensor activation times, $t_{LAV,i}$, for the five sensors nearest to the fire (i = 1 to 5). Random and systematic errors were added to the LAVENT simulated sensor activation times, to produce the corrupted sensor activation times, $t_{a,,i}$, using equation (5). The inverse problem solution algorithm was then employed, using the corrupted sensor activation times, $t_{a,,i}$, as data, to predict a fire location and heat release rate, $(x_{pred}, y_{pred}, \alpha_{pred})$.

The accuracy of the inverse problem solution algorithm was scored by calculating the errors in the algorithm's predictions of the fire location and heat release rate. The location error, ε_{loc}, was defined to be the distance between the fire location (x_{pred}, y_{pred}) predicted by the inverse problem solution algorithm and the location (x_{sim}, y_{sim}) originally selected to produce the simulated sensor times to activation:

$$\varepsilon_{loc} = \sqrt{\left(x_{pred} - x_{sim}\right)^2 + \left(y_{pred} - y_{sim}\right)^2} \qquad (7)$$

where ε_{loc} is measured in centimeters. For a perfect fire detection system with no error, ε_{loc} = 0 cm. The heat release rate error ratio, ε_Q, was defined to be the ratio of the heat release rate of the fire, predicted by the inverse problem solution algorithm, $Q_{pred}(t_{a,5})$, over the heat release rate of the fire originally simulated, $Q_{sim}(t_{a,5})$, where both heat release rates are calculated at the time of the activation of the fifth sensor:

$$\varepsilon_Q = Q_{pred}\left(t_{a,5}\right) \Big/ Q_{sim}\left(t_{a,5}\right) \qquad (8)$$

The heat release rate error ratio is dimensionless. Note that as the predicted heat release rate, $Q_{pred}(t_{a,5})$, and the simulated heat release rate, $Q_{sim}(t_{a,5})$, diverge, the value of heat release rate error ratio, ε_Q , shifts away from unity. Heat release rate error ratios less than unity mean the inverse problem solution algorithm has underpredicted the fire size, while ratios greater than unity mean the algorithm has overpredicted fire size.

The inverse problem solution algorithm was run using data from 1000 different simulated fires to provide an ensemble of results at each set of test conditions. The location, (x,y) of each of the simulated fires was randomly chosen, while the growth rate, α, of the fires was kept constant over all of the 1000 simulated runs. A set of test conditions consisted of the specified magnitudes of random error and systematic error added to the simulated fire data, along with the fire growth rate. Since random error is determined by the standard deviation, σ, of the Gaussian distribution $G(\sigma)$, while systematic error is controlled by the constants b and c in Eq. (5) a test condition is specified by the set of parameters: (α, σ, b, c). Location and heat release rate error statistics for each test condition were determined from the ensemble of errors resulting from the 1000 simulated test fire runs.

2.2.4 Evaluation of the Inverse Problem Solution Algorithm: Interpolated Fire Measurements

A second test of the inverse problem solution algorithm was run using data interpolated from experimental measurements given in Ref [9]. The test was run by first

randomly selecting a fire location, (x_{sim}, y_{sim}), in the range $0 < x_{sim} < d$, $0 < y_{sim} < d$. The fire growth rate, $\alpha_{sim} = 0.0426\ \text{kWs}^{-2}$ was set by the growth rate of the compartment fire from which the measurements were taken. The transient temperature history at the compartment ceiling for the given fire location and growth rate was determined using the method outlined in section 2.3.2. Transient temperatures found using Eq. (6) and the pdf determined from measurement residuals were then used to determine sensor activation times, $t_{LAV,i}$, for the five sensors nearest to the fire (i = 1 to 5). The inverse problem solution algorithm was then employed, using the sensor activation times, $t_{a,,i}$, as data, to predict a fire location and heat release rate, $(x_{pred}, y_{pred}, \alpha_{pred})$.

The accuracy of the inverse problem solution algorithm in locating and sizing fires using the interpolated data was assessed in the same way the first test was scored. The location error, ε_{loc}, was taken to be the distance between the fire location (x_{pred}, y_{pred}) predicted by the inverse problem solution algorithm and the location (x_{sim}, y_{sim}) originally selected to produce the simulated sensor times to activation (See Eq. (6)). The heat release rate error ratio, ε_Q, was taken to be the ratio of the heat release rate of the fire, predicted by the inverse problem solution algorithm, $Q_{pred}(t_{a,5})$, over the heat release rate of the fire from which the data were taken, $Q_{act}(t_{a,5})$:

$$\varepsilon_Q = Q_{pred}\left(t_{a,5}\right) \Big/ Q_{act}\left(t_{a,5}\right) \qquad (9)$$

Here both heat release rates were determined for the time of the activation of the fifth sensor.

The inverse problem solution algorithm was run using data for fires at 1000 different locations to provide an ensemble of results. Location and heat release rate error statistics for each test condition were then determined from the ensemble of errors resulting from the 1000 simulated test fire runs.

2.3 Results: Computer Simulated Fire Data

2.3.1 Fire Location Accuracy

The accuracy of the inverse problem solution algorithm in locating fires can be assessed by referring to Figs. 2 and 3, where statistics on fire location error from 1000 simulated test fires are shown. Consider first Figs. 2a and b, where the effect of random errors and systematic errors on the inversion algorithm's accuracy in predicting fire location is illustrated. In the figures, probability density functions for location error are shown for both slow-growing ($\alpha = 2.98$ Ws^{-2}) and fast-growing ($\alpha = 42.6$ Ws^{-2}) fires given. Location errors are reported as the distance between predicted and actual fire locations, and given in centimeters.

The effect of random error is shown in Fig.2a. In that figure, where no systematic error has been added (LAVENT is assumed to be a "perfect" fire model.), probability density functions of location error for simulations of fires with no random error ($\sigma = 0$ sec) and with moderate random error ($\sigma = 5$ sec), are given. As expected, errors in the fire location predicted by the inverse problem solution algorithm increase as random measurement errors increase. The effect is seen to be greater for fast-growing fires than for slow-growing fires.

Figure 2b shows the effect of systematic or model error on the accuracy of the inversion algorithm to predict the fire location. Pdf's of location error are given for cases of fire data with systematic error corresponding to $a = 0$s, $a = 40$s, $b = 0$, and $b = 0.6$ with an added random error of $\sigma = 5$ s. Location errors are seen to be larger for fast-growing fires than for slow-growing fires as in Fig. 2a. However, in contrast to the previous case, fire location errors do not increase as systematic model error increases. In fact, for the fast growing fires, location errors decrease slightly when the parameter b is increased. This conclusion can be seen more clearly in Figs 3a and 3b

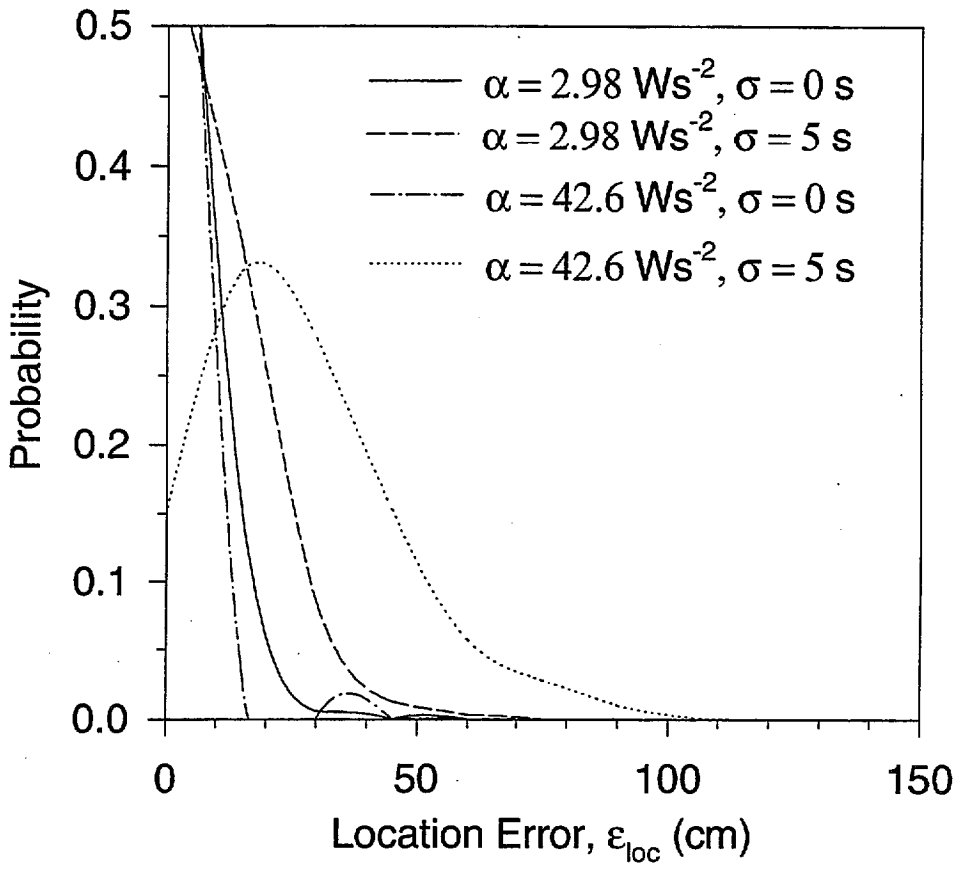

Fig. 2 a. Location error PDF's for slow and fast-growing fires:α = 2.98 Ws^{-2} and α = 42.6 Ws^{-2} at two levels of random error: σ = 0.0 and σ = 0.5, and no systematic error.

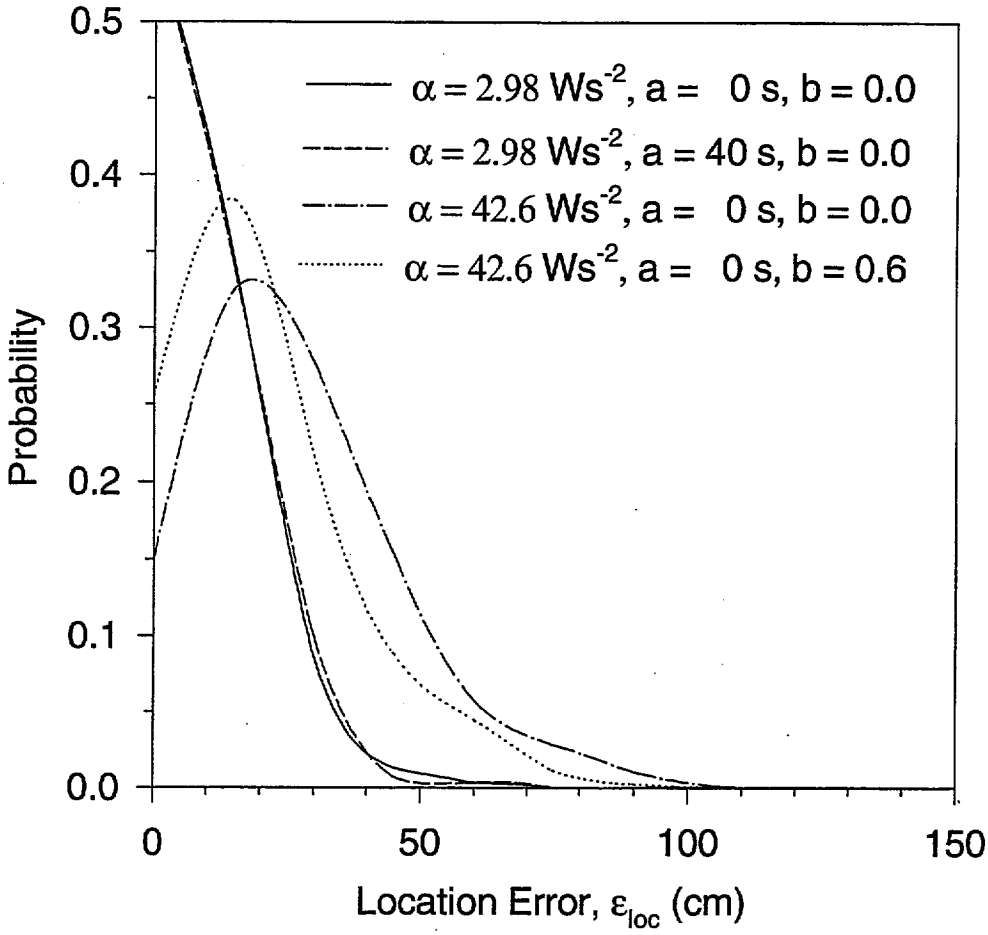

Fig. 2 b. Location error PDF's for slow and fast-growing fires: $\alpha = 2.98$ Ws^{-2}and $\alpha = 42.6$ Ws^{-2}, at three levels of systematic error: a = 0, b=0.0; a = 40, b = 0.0; a = 0, b = 0.6, and random error $\sigma = 5$ s.

In Figs. 3a and b both the median error and the 95% confidence intervals about the median error in fire locations predicted by the inverse problem solution algorithm are plotted versus random error standard deviation, σ. Only results for fast-growing fires (α = 42.6 Ws^{-2}) are shown. The median location error represents an error greater than the location errors found for 50% or 500 out of 1000 test fires. Likewise, the 95% confidence interval represents a location error greater than the location errors for 95% or 950 out of 1000 fires in a test run. In Fig. 3a location error is plotted for three cases of systematic error: a = 0, 20, 40 s with b = 0.0 while in Fig, 3b location error is plotted for three other cases of systematic error: a = 0 s with b = 0, 0.2, 0.4. Both figures clearly demonstrate that varying systematic error by changing parameters a and b has little effect on either the median or the 95% confidence intervals for location errors. On the other hand, increasing the random error standard deviation, σ, causes monotonic increases in both the inversion algorithm's median location error and 95% confidence interval on location error.

The insensitivity of inverse algorithm location error to systematic model error and the sensitivity of the location error to random measurement error are both consequences of the fact that the algorithm predicts fire location primarily on the basis of the order in which sensors are activated. For example, the inverse algorithm will always predict the fire to be

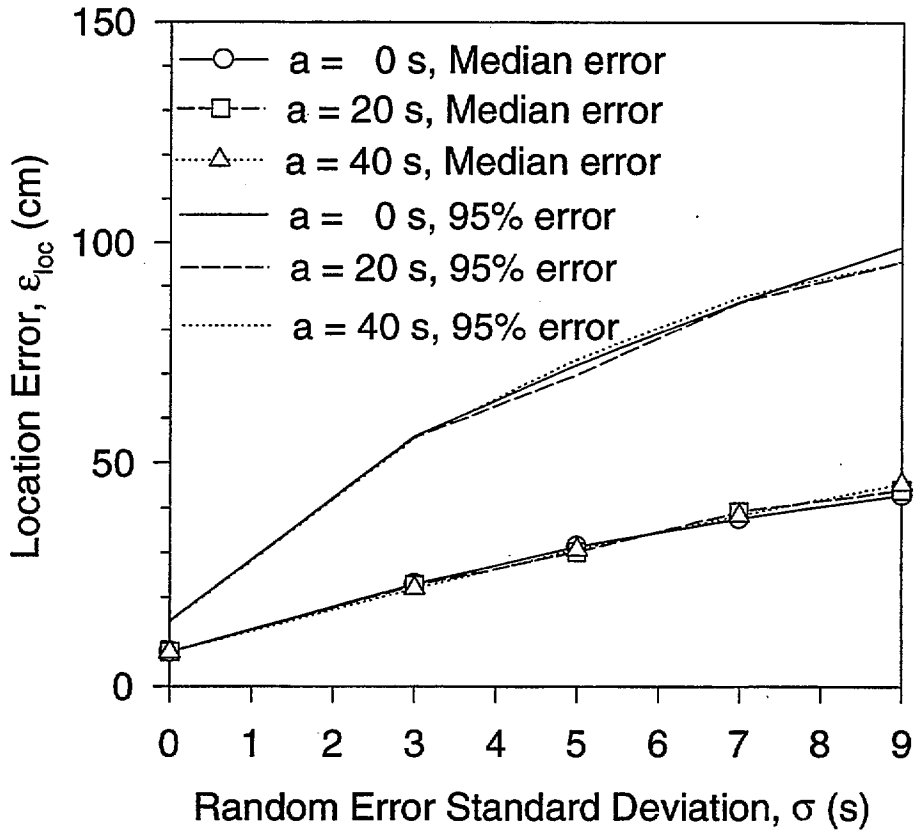

Fig. 3 a. Median location error with 95% confidence interval versus random error, for fast-growing fires: $\alpha = 42.6\ Ws^{-2}$, for three levels of systematic error: a = 0 s, b = 0.0; a = 20 s, b = 0.0; and a = 40 s, b = 0.0.

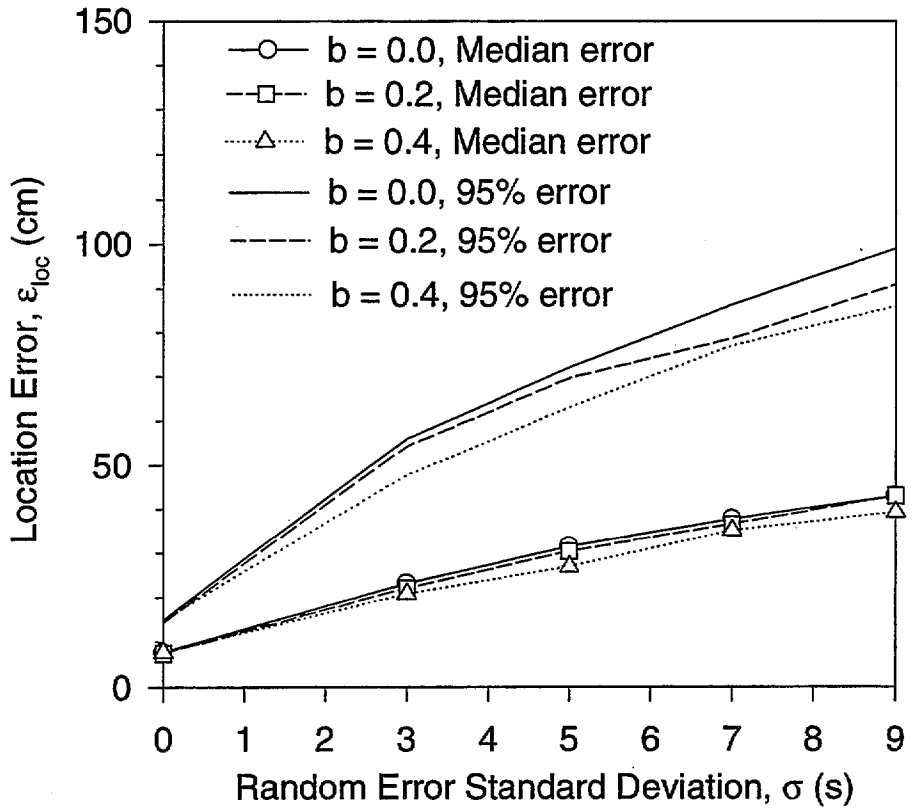

Fig. 3 b. Median location error with 95% confidence interval versus random error, for fast-growing fires: $\alpha = 42.6\ Ws^{-2}$,for three levels of systematic error: a = 0 s, b = 0.0; a = 0 s, b = 0.2; and a = 0 s, b = 0.4.

closest to the sensor which is activated first, the fire to be next closest the sensor activated second, and so on. The algorithm predicts fire location secondarily on the relative elapsed times between activation of sensors. That is the longer it takes for a sensor to activated, the farther that sensor must be from the fire. All radially symmetric compartment fire models will predict the same sequence of sensor activations for a given fire location. All radially symmetric compartment fire models will predict that the greater the distance from the fire to any given sensor the greater the elapsed time until the sensor is activated. For these reasons, the particular fire model used in the inverse problem solution algorithm will have little effect on the fire location predicted. In the same way, systematic errors in the fire model will have little effect on fire location errors, as seen in Figs. 3a and b.

The effect of random errors is quite different. Random measurement errors will cause the relative times of activation of sensors to vary from their "true" values. A random measurement error causing the apparent activation time of a sensor to be sooner than the actual elapsed time will shift the predicted fire location closer to that sensor. A random error causing a sensor activation time to appear later than the actual time will shift the predicted fire location away from that sensor. In the case of large random measurement errors the sequence of two sensor activations may even be reversed. The increase in fire location error with increased random measurement errors seen in Figs. 3a and b reflects these mechanisms.

2.3.2 Fire Heat Release Rate Accuracy

The effect of random and systematic errors on the accuracy of the inversion algorithm in predicting fire heat release rates for fast and slow-growing fires is shown in Figs. 4a and b. In the figures, heat release rate error ratio probability density functions are given, where heat release rate error ratio is reported as the heat release rate predicted by the inversion algorithm, divided by the actual fire's heat release rate, at the time of the fifth sensor activation. The effect of random error is shown in Fig. 4a where heat release rate error ratio pdf's are given for fire data with $\sigma = 0$ s and 5 s with no systematic error (perfect fire model). Increasing random measurement error is seen to have little effect on the peak of

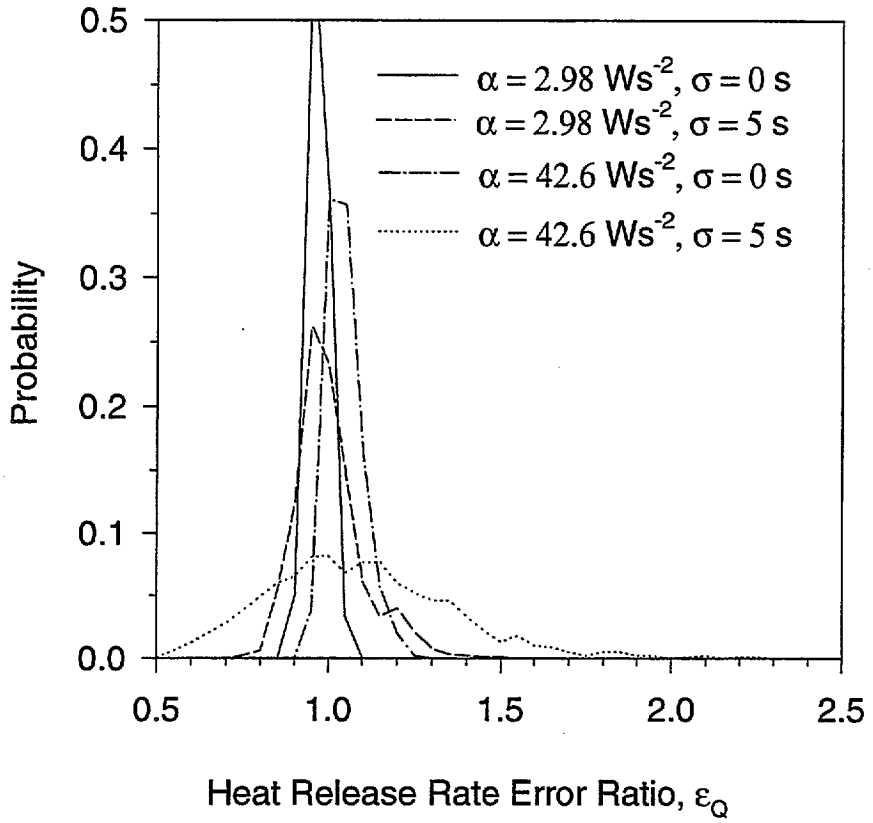

Fig. 4 a. Heat release rate error PDF's for slow and fast-growing fires: $\alpha = 2.98$ Ws^{-2} and $\alpha = 42.6$ Ws^{-2} and two levels of random error: $\sigma = 0$ s, and $\sigma = 5$ s, with no systematic error.

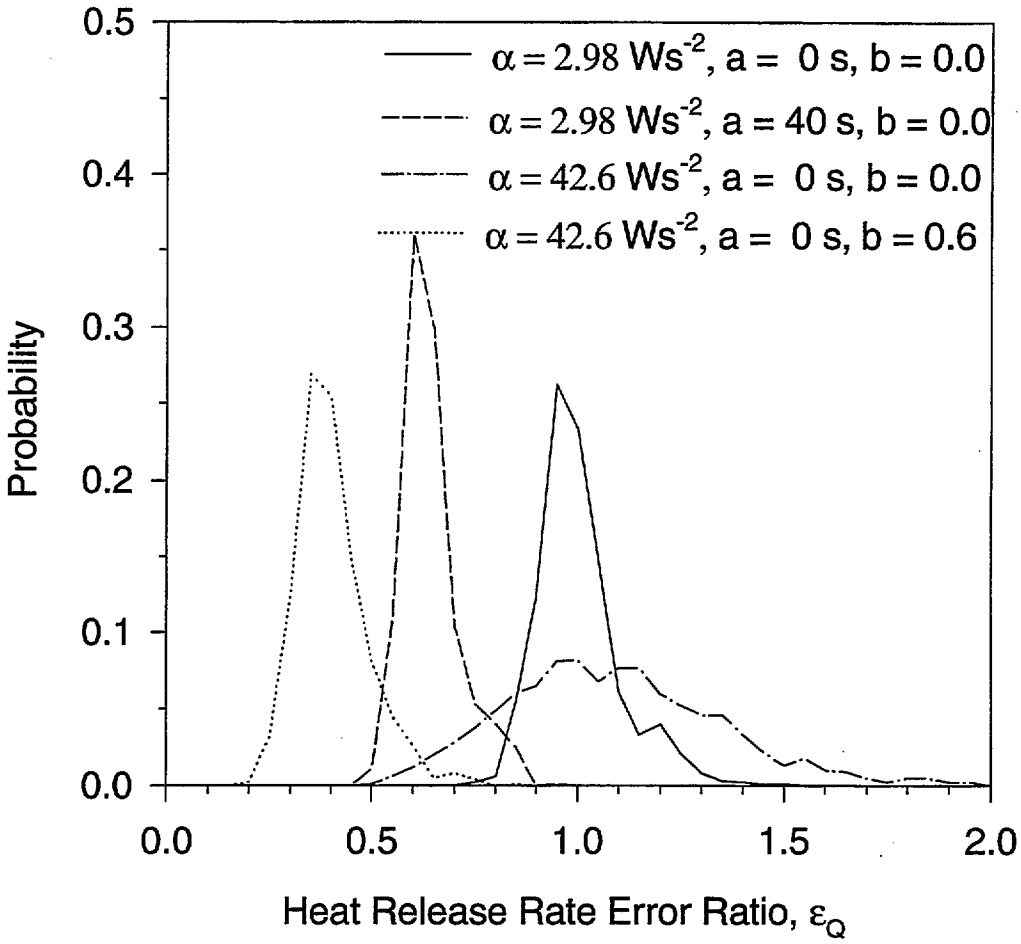

Fig. 4 b. Heat release rate error ratio PDF's for slow and fast-growing fires: $\alpha = 2.98$ Ws^{-2} and $\alpha = 42.6$ Ws^{-2}, at systematic error: a = 0 s, b = 0.0; a = 40 s, b = 0.0; a = 0 s, b = 0.6 and random error $\sigma = 5$ s.

the heat release rate error ratio pdf, while causing the width of the pdf to grow. The increase in pdf width is larger for the fast-growing fires.

The effect of systematic error is shown in Fig. 4b. In the figure, heat release rate error ratio pdf's are given for cases of systematic error corresponding to $a = 0$ s, $a = 40$ s, $b = 0$, and $b = 0.6$, for fire data with added random error of $\sigma = 5$ s. Increasing systematic error causes the peak of the heat release rate error ratio pdf to shift away from unity to smaller values. Again, the shift is greater for fast-growing fires. Interestingly, the width of the pdf appears to decrease with increasing systematic error. However, the width of the heat release rate error ratio pdf normalized by the mean value of the heat release rate error ratio remains constant. This can be seen in Figs. 5 a and b.

Figures 5a and b give semi-logarithmic plots of median error and 95% confidence intervals about the median error for predicted heat release rate error ratio versus systematic error. In Fig. 5a heat release rate error ratio is plotted on a log scale against the systematic error parameter, a, ($b = 0$) for three cases of random error: $\sigma = 0, 5, 9$ s. In Fig, 5b heat release rate error is plotted on a log scale against the systematic error parameter, b, ($a = 0$) for the same three cases of random error: $\sigma = 0, 5, 9$ s. In both figures results are shown for fast-growing fires ($\alpha = 42.6$ Ws^{-2}) only.

Figures 5a and b show a very different behavior for heat release rate errors than Figs. 3a and b showed for location errors for the inverse problem solution algorithm. Recall that Figs. 3a and b showed that location errors were sensitive to random measurement errors but insensitive to systematic errors in the fire model. Figs. 5a and b show that median errors in heat release rate are sensitive to systematic model error (changes in either a or b) and are insensitive to random measurement error (changes in σ). In contrast, the 95% confidence intervals on heat release rate error, as seen on the semi-log plots, are insensitive to systematic model error (changes in a or b) and are sensitive to random measurement error (changes in σ). In other words, increasing systematic model error (parameters a and b) will cause the peak of the heat release rate error pdf to shift to successively smaller values of ε_Q, where the smaller the value of ε_Q, the more the inverse problem solution algorithm is

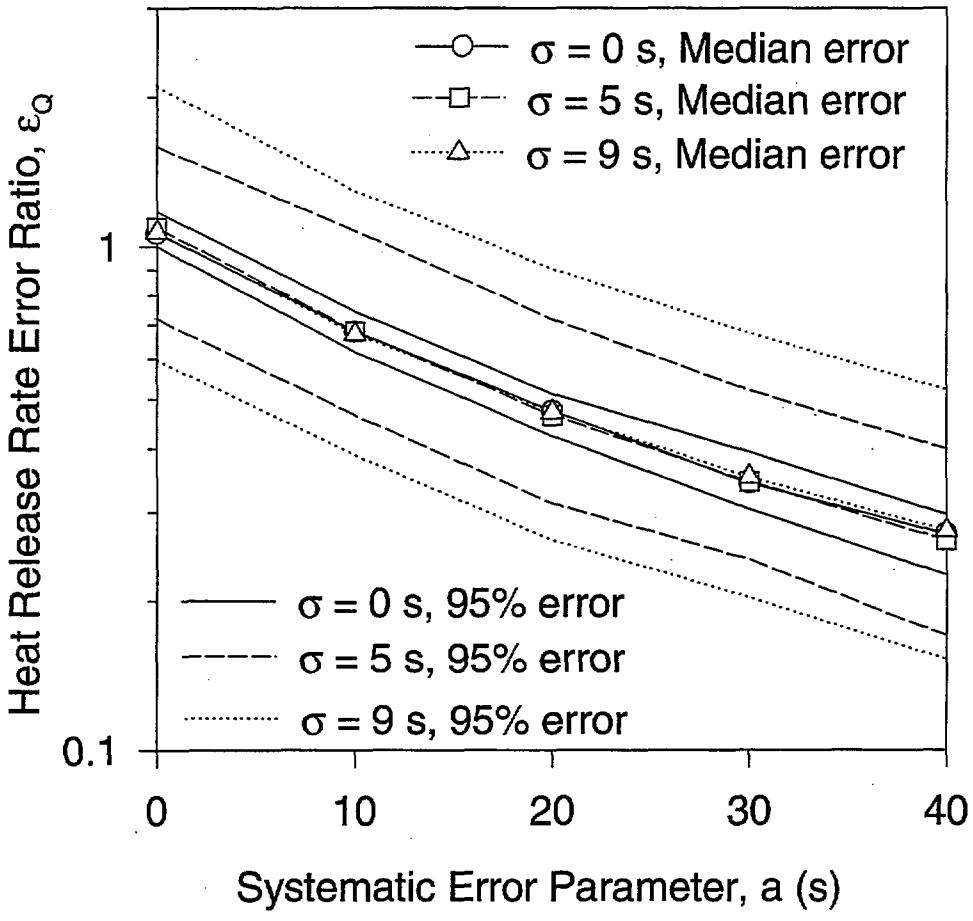

Fig. 5 a. Median heat release rate error ratio with 95% confidence intervals versus systematic error parameter, a, for fast-growing fires, a = 42.6 Ws^{-2} for three levels of random error: σ = 0 s, σ = 5 s, and σ = 9 s.

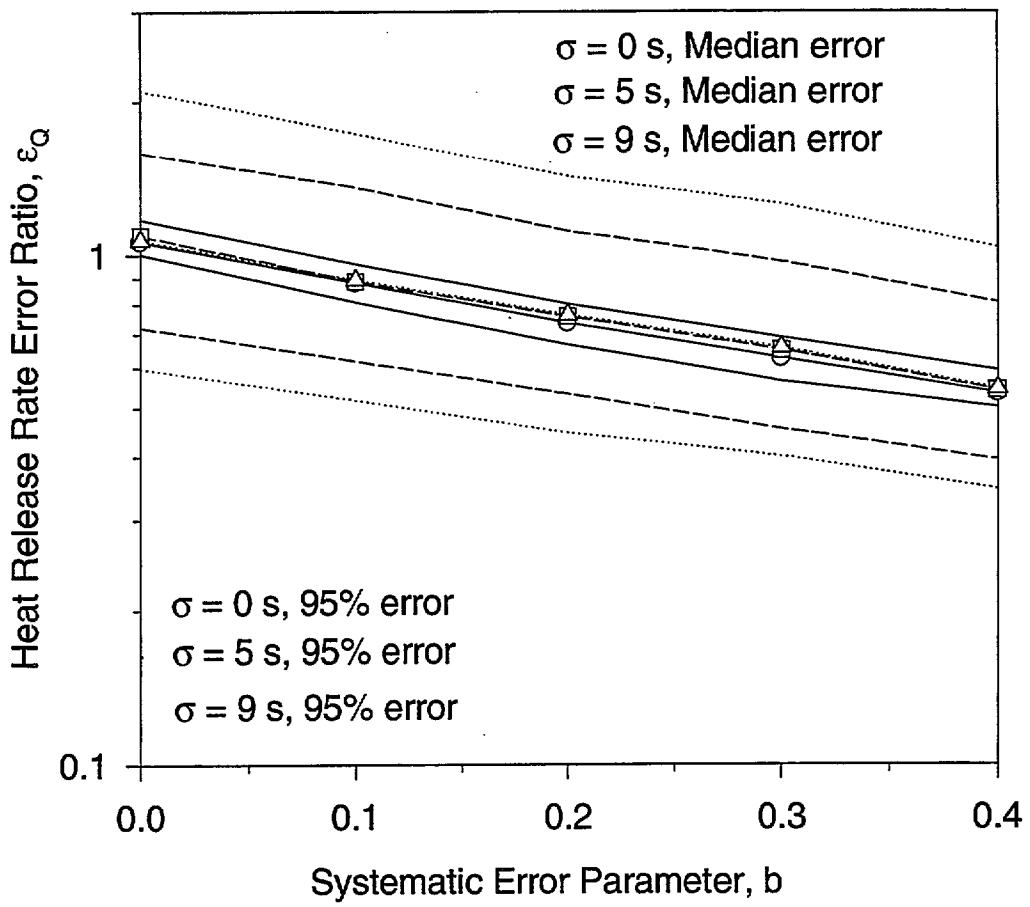

Fig. 5 b. Median heat release rate error ratio with 95% confidence intervals versus systematic error parameter, b for fast-growing fires, $\alpha = 42.6\ Ws^{-2}$, for three levels of random error: $\sigma = 0$ s, $\sigma = 5$ s, and $\sigma = 9$ s.

underpredicting the fire size. At the same time, increasing systematic model error will have no effect on the width of the pdf as seen on the semi-log plot, where a constant width implies a constant ratio between the median error ratio and the 95% error ratio. In contrast, increasing random measurement error will have no effect on the position of the peak of the heat release rate error pdf, while causing the width of the pdf to increase.

The accuracy of fire heat release rates predicted by the inverse problem solution algorithm is tied closely to the accuracy of the forward model (in the present case: LAVENT) used by the algorithm. The accuracy of fire locations predicted by the inverse algorithm does not depend on the accuracy of the forward model. If the forward model overpredicts compartment ceiling temperatures then the inverse problem solution algorithm will consistently underpredict fire heat release rate, but may still accurately predict the fire location. This is precisely the meaning of Figs. 3a, b and 5a, b. The dependence of fire heat release rate predictions on forward model accuracy, in contrast to the independence of fire location predictions from forward model accuracy, makes the determination of fire size a much more difficult task than the determination of fire location, for a practical fire detection system.

2.3.3 Fire Detection Speed

The speed with which the proposed fire detection system can locate and size a fire is of interest. Figure 6 shows probability density functions for activation times of the first and fifth sensors for a slow-growing fire ($\alpha = 2.98$ W/s^2) and a fast-growing fire ($\alpha = 42.6$ W/s^2) for 1000 test runs. Upon activation of the first sensor the system has its first evidence of the fire. Upon activation of the fifth sensor the inversion algorithm has sufficient information to locate the fire. The slow-growing fire is seen to be first detected within two minutes and located and sized within three minutes. The fast-growing fire is first detected within 30 seconds and located and sized within 50 seconds.

Figure 6 also demonstrates why location and heat release rate errors are greater for fast-growing fires than for slow-growing fires given equal magnitudes of random and systematic error. Consider, for example a case in which sensor activation times for both fast

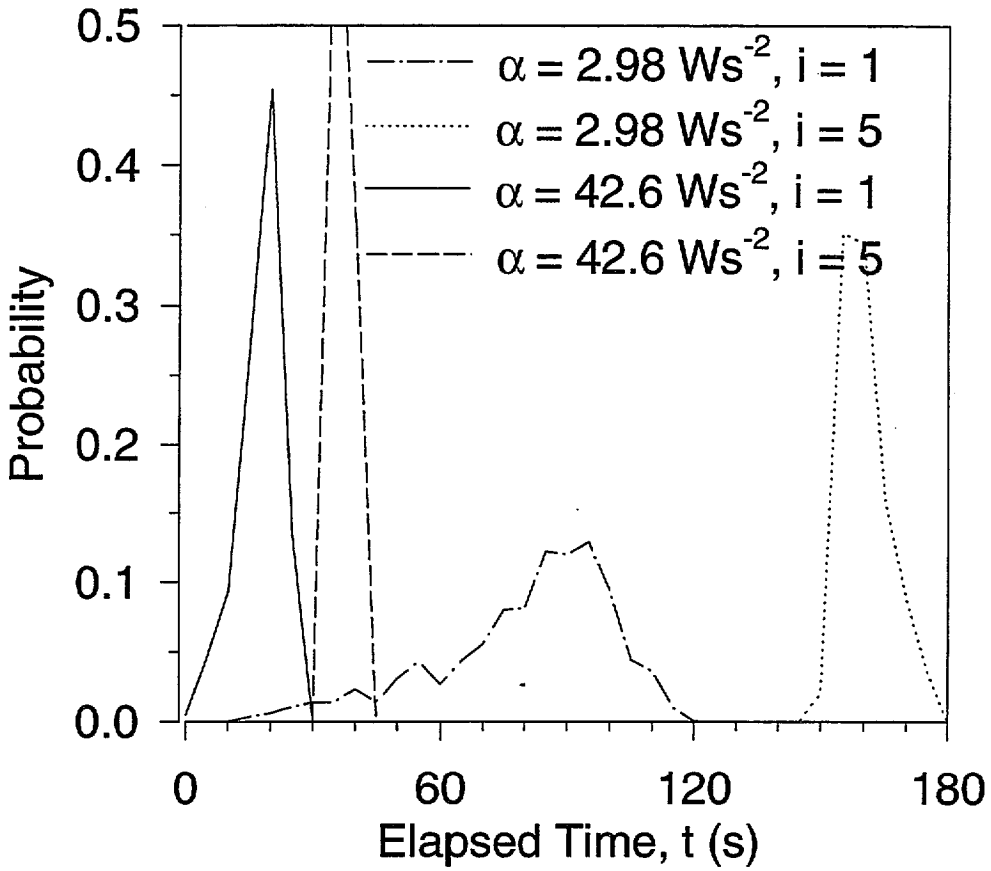

Fig. 6. Sensor time to activation PDF's for first and fifth sensors

and slow-growing fires have associated with them random error with $\sigma = 5$ s. The mean time of activation of the first sensor is 19 s for the fast-growing fire and 37 s for the slow-growing fire. The random error then is 26% of the activation time for the fast-growing fire but only 14% of the activation time for the slow-growing fire. Likewise a systematic error consisting of a constant bias of a = 5 s would constitute a much larger fraction of the sensor activation times for fast-growing fires than for slow-growing fires. It is the ratio of activation time errors to the activation times themselves and not the absolute magnitude of the errors which controls the accuracy of the inverse problem solution algorithm. This ratio will always be larger for fast-growing fires than for slow-growing fires given equal random and systematic errors. Figures 2a and b and 4a and b reflect this fact.

2.4 Results: Interpolated Fire Measurements

The validity of the use of simulated fire data in the evaluation of the inverse problem solution algorithm was investigated. Results of the evaluation using simulated data were compared to an evaluation using data interpolated from experimental measurements taken in a large-scale compartment fire test.

The method of interpolation of data from actual measurements using the correlation given as Eq. (6) in conjunction with the time residual pdf has been described in section 2.3.2. It is important to emphasize here that although the interpolated sensor activation time data are not experimental measurements, the data were developed directly from, and closely resemble, the original measurements. To judge how closely the interpolated data resemble the original data from Ref. [9], a comparison between some of the original measurements and the interpolated data is given in Fig. 7. In the figure, data from Ref. [9] in the form of time versus temperature measurements for three radial locations on the ceiling above a fast-growing ($\alpha = 42.6$ Ws^{-1}) compartment fire are plotted with filled symbols. On the same figure, data interpolated from the experimental measurements using the method of section 2.3.2, are plotted with open symbols. The comparison between the interpolated data and the original measurements from which they were derived is seen to be quite good.

Results of the evaluation of the inverse problem solution algorithm based on

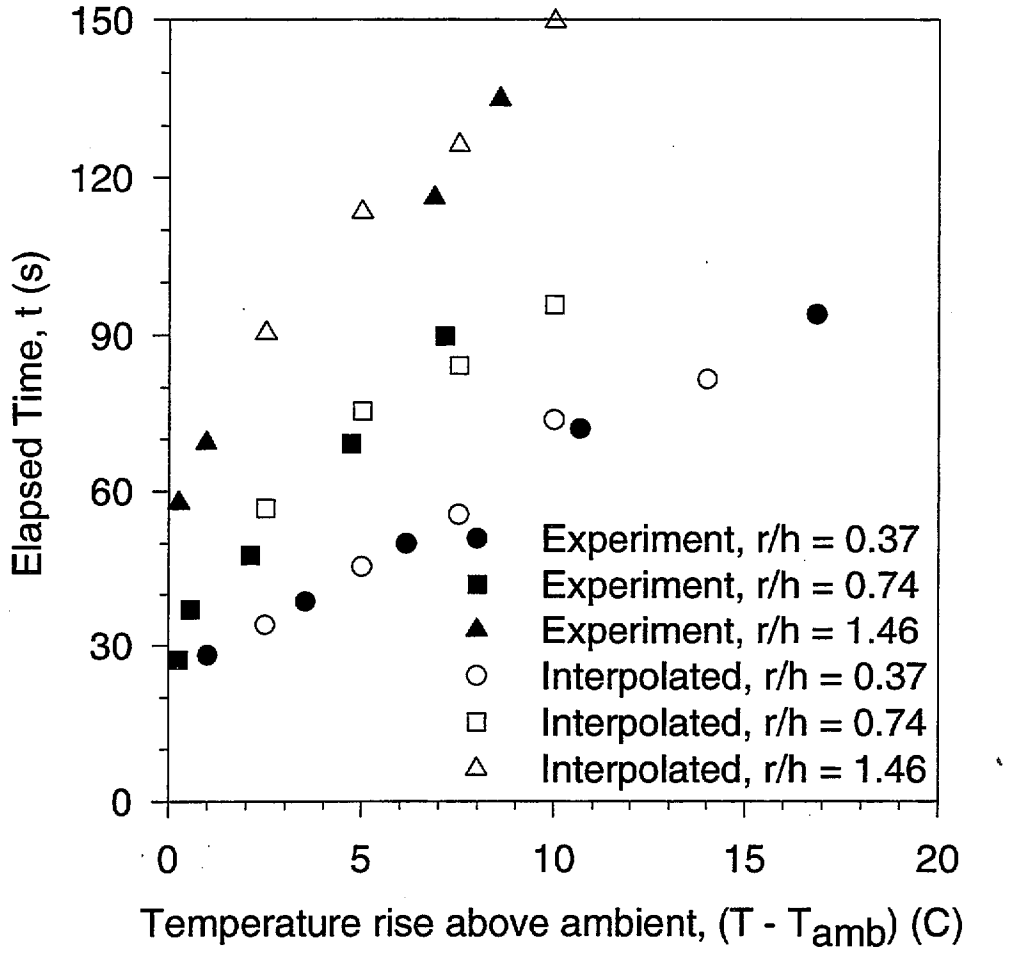

Fig. 7 Comparison of experimental measurements taken from Ref. [9] and interpolated data produced using Eq. (6) and residual probability distribution function.

interpolated data, similar to the data shown in Fig. 7, are given in Figs. 8a and b, alongside results from an evaluation using computer simulated data. The figures show pdf's for location errors and heat release rate error ratios for the inverse problem solution algorithm, when locating and sizing 1000 randomly-located, fast-growing fires ($\alpha = 42.6$ Ws^{-1}). Solid lines show results from the evaluation using interpolated fire data. Dashed lines show results from the evaluation using computer simulated fire data. The computer simulated data, produced using LAVENT contains random error with $\sigma = 5$ s and systematic error with $a =$ 20 s and $b = 0.20$. Figures 8a and b show that location errors and heat release rate error ratios found from an evaluation of the inverse algorithm based on LAVENT synthesized data are essentially indistinguishable from results of an evaluation of the inverse algorithm based on fire data interpolated from experimental measurements. In short, the use of computer simulated data will lead to realistic and useful estimates of the fire detection system's accuracy, as long as random and systematic errors of appropriate magnitude are included in the data.

The magnitudes of location and heat release rate ratio errors seen in Figs. 8 a and b are instructive. Recall that the figures are based on the assumption of a fast-growing fire in a large (20 x 20 x 3 m) warehouse. Under these conditions, the inverse problem solution algorithm was able to locate 95% of the fires within 70 cm, (2/3 d) and 50% within 30 cm (1/3 d). Location accuracy for the inverse problem solution algorithm is quite good. The inverse algorithm was able to determine the heat release rate of 95% of the fires to within a factor of five ($\varepsilon_Q = 0.2$) and 50% of the fires within a factor of three ($\varepsilon_Q = 0.33$). Accuracy of fire heat release rate is not as good. However, the heat release rate error ratios given in Fig. 8b are probably artificially low. The values of ε_Q (where $\varepsilon_Q = Q_{pred}/Q_{act}$) are too low because the values of actual heat release rate, Q_{act}, on which they are based are most likely too high. The values of actual heat release rate taken from Ref. [8] were determined by multiplying a measured rate of change of fuel mass by an estimated heat of combustion for the fuel. As a consequence a combustion efficiency of less than 100% in the test fire would result in an overestimate of Q_{act} and an underestimate of ε_Q.

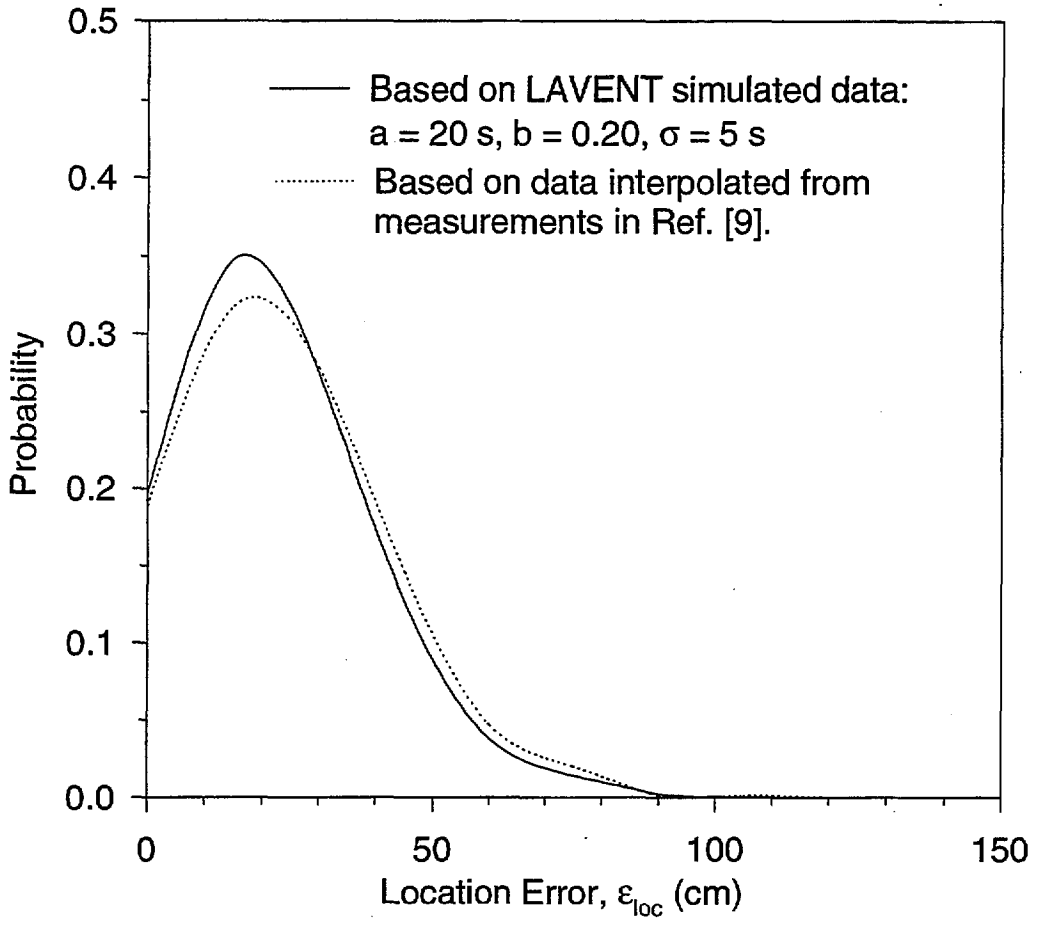

Fig. 8 a. Comparison of location errors determined using LAVENT simulated data and data interpolated from measurements reported in Ref. [9]. LAVENT data simulated with systematic error: a = 20 s, b = 0.2, and random error: σ = 5 s.

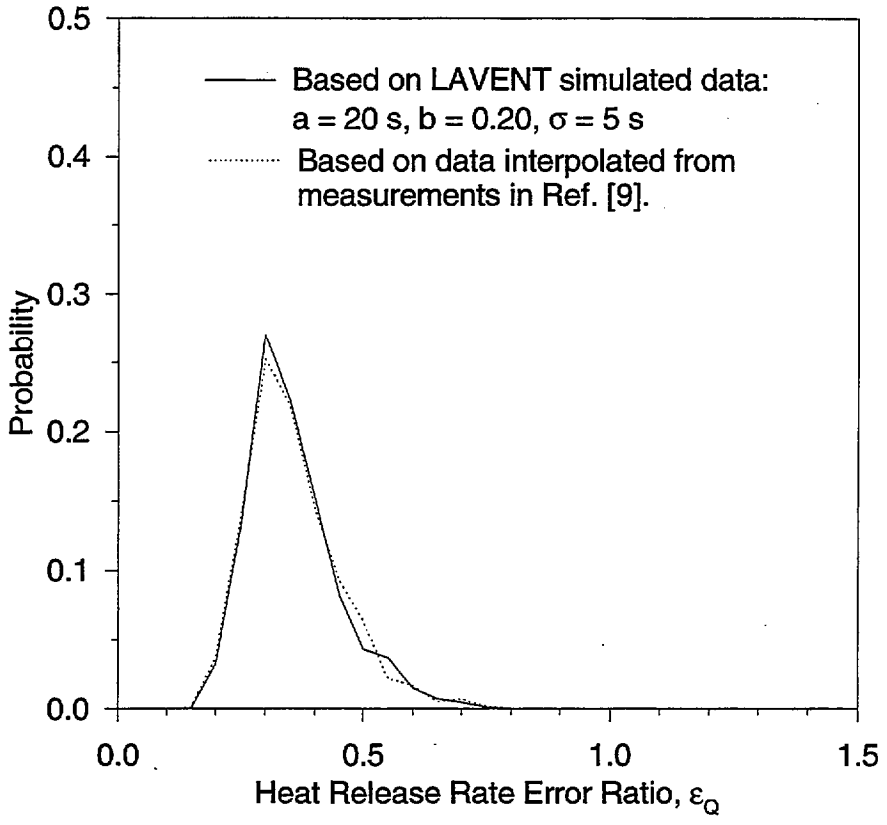

Fig. 8 b. Comparison of heat release rate error ratios determined using LAVENT simulated data and data interpolated from measurements reported in Ref. [9]. LAVENT data simulated with systematic error: a = 20 s, b = 0.2, and random error: σ = 5 s.

3 Experiment: The Prototype Video Fire Detection System

A prototype video fire detection system employing the inverse problem solution algorithm to locate and size fires was assembled. The operation of the video fire detection system is illustrated in Fig. 9. A black and white video camera monitors passive sensors placed in a regular array on the ceiling of the compartment to be protected. An accidental fire has ignited and begins to send a plume of hot smoke and combustion gases to the ceiling of the compartment. The sensors are each composed of black and white targets and a sheet of temperature-sensitive, color-changing material, and serve two functions. The temperature-sensitive material in the sensors visibly changes color when the sensors reach their activation temperature. This color change enables the video system to track the advance of hot combustion gases across the ceiling. The black and white targets in the sensors serve as reference standards against which to measure the turbidity of smoke coming between the sensors and the video camera. Changes in the relative brightness of black and white targets on sensors obscured by smoke, enable the video system to track the advance of a fire's smoke plume. As sensors reach their activation temperature and change color, the video system records the location of the sensor and its time of activation. Once the temperature-sensitive material on five sensors has been activated, the personal computer based inverse problem solution algorithm uses the measured times of activation as data to determine the most probable location and heat release rate of the accidental fire.

The design of the video fire detection system can be best understood in terms of its two major components. The first major component is the video data gathering hardware, composed of the distributed array of sensors, the black and white video camera, and the frame grabber. The video data gathering hardware supplies the fire detection system with sensor time of activation data and line of sight optical density data. The second major component of the fire detection system is the personal computer based inverse problem solution algorithm which locates and sizes the fire.

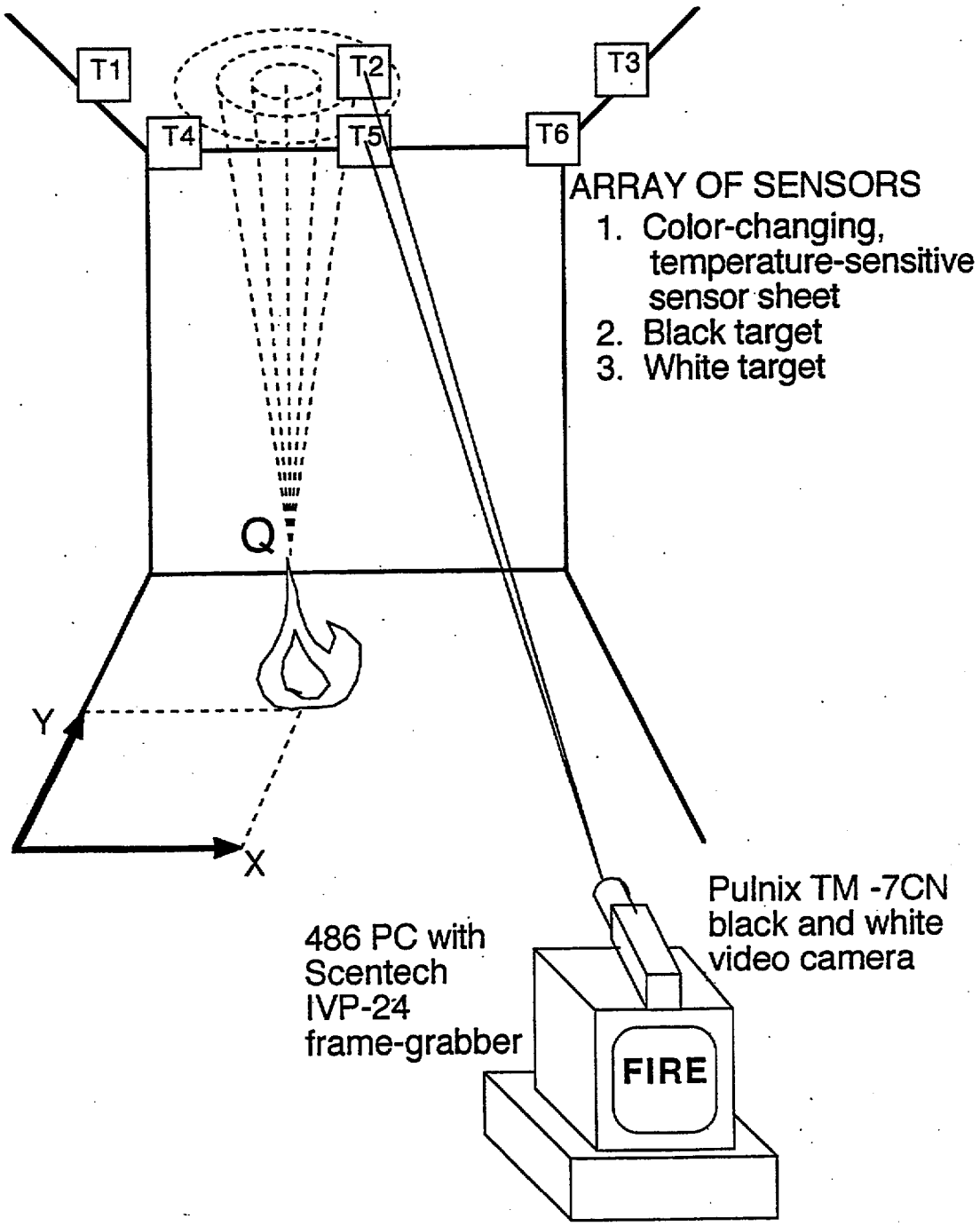

Figure 9. The operation of the video fire detection system.

3.1 Video Data Gathering Hardware

The video camera used in the present work is a black and white Pulnex TM-7CN CCD camera equipped with a telephoto lens. Video images are digitized using a Scentech IV-P24 color frame grabber (using only one channel, for black and white images) and passed on to a 30Mhz, 486 personal computer. This system is able to digitize and evaluate images from the video camera every 0.8 seconds, allowing for essentially continuous, real-time monitoring. The images digitized by the frame grabber and evaluated by the personal computer consist of 640 x 480 arrays of pixels with integer gray-scale values running from 0 (black) to 255 (white). Color changes in activated sensors appear in the digitized video images of sensors as changes in the gray-scale values of the pixels making up the images. To determine a color change in a sensor, the system calculates the average of the gray-scale values of twenty pixels in a sensor image. An average over twenty pixels is used to eliminate errors due to electronic noise. A change in gray scale of 15 out of 255 or 6% of the full gray-scale range is taken as the threshold value for sensor activation. The times of activation of the sensors are reckoned by reference to the personal computer's built in clock, and are determined to the nearest second.

The sensors are 10 cm by 30 cm flat sheets composed of three, side by side, 10 cm by 10 cm areas: a black target, a white target, and a temperature-sensitive, color-changing sheet. The size was chosen to ensure that each area of the sensor images would be made up of more than twenty pixels, even when the sensors were more than 10 m from the video camera. Two kinds of temperature-sensitive materials were tested for use in the sensors.

The first batch of color-changing sheets was made by painting flat black paint on 0.1 mm plastic sheets and then painting over the black paint with a second coat of paint consisting of microencapsulated thermochromic liquid crystals (TLC) suspended in a clear binder. The TLC paint is transparent until it reaches the temperature of 30 C. Below 30 C the sheet appears black. As the temperature of the TLC paint rises from 30 C to 35 C the TLC paint selectively reflects light in a narrow wavelength band, with the wavelength band being a function of temperature. At 30 C the TLC paint reflects long wavelength light (red) and then reflects progressively shorter wavelength light until it reaches 35 C when blue is

seen. As a result, the sensor appears to run through the colors of the visible spectrum. Above 35 C the TLC paint is again transparent, and the sheet appears black. Since the TLC color change is completely reversible, sensors using TLC can be activated many times.

A second batch of color-changing sheets was made by painting the same flat black paint on 0.1 mm plastic sheets and then painting over the black paint with a second coat of Omegalaq, a low-temperature melt paint material obtained from Omega Engineering Inc. Below its melting point at 38 C the melt paint is light purple. Upon melting the melt paint becomes semi-transparent, revealing the black undercoated paint.

In all sensors the black target was made by painting the same flat black paint on 0.1 mm plastic sheets. The appearance of the black target was thus identical to the TLC color-changing sheet before activation, and nearly identical to the melt paint color-changing sheet after activation. This equivalence in appearance allows sensor activation to be determined by comparing the average gray-scale pixel value of the temperature-sensitive, color-changing sensors against the gray-scale pixel value of the black target. The white target was made of plain white poster board.

3.2 Inverse Problem Solution Software

The inverse problem solution algorithm employed in the prototype fire detection system is described in detail in section 2.1. The algorithm is implemented in the event that the video data gathering system registers the color change, or activation of five adjacent sensors. As each sensor is activated, the personal computer records both the location and the activation time (clock time) of the sensor. Four elapsed times to activation are calculated for the second through the fifth sensors by subtracting their activation times from the activation time of the first sensor.

To determine the fire's location and heat release rate, the inverse problem solution algorithm compares the four measured activation times with activation times predicted by the zone fire model LAVENT [8] for various fire scenarios. More specifically, the algorithm calculates the sum of squares of differences between the measured activation times and predicted activation times computed by LAVENT for fires at various locations and with

various growth rates. The fire scenario, or fire location and growth rate, which minimizes the sum of squares of the differences between measured and predicted times to activation is taken as representing the most probable fire location and growth rate.

3.3 Evaluation of the Prototype Fire Detection System

The evaluation of the prototype video fire detection system focuses on three issues: the ability of the video data gathering system to collect useable data from an array of sensors under fire conditions (including the presence of smoke), the ability of the inverse problem solution algorithm to use data gathered by the video system to locate and size a real flame source, and the ability of the fire detection system to locate a smoke plume. To explore these issues, three separate tests were run.

The first test evaluated the ability of the video data gathering system to detect the activation of the temperature-sensitive, color-changing sensors under a range of lighting conditions and in the presence of smoke. In addition, the system's ability to detect smoke and to measure the optical density of the smoke was evaluated. The second test evaluated the accuracy of the prototype video detection system in determining the location and heat release rate of 2.4 kW and 4.8 kW flame sources placed in a test enclosure. In this test the inverse problem solution algorithm operated on data supplied to it by the video camera monitoring temperature-sensitive, color-changing sensors exactly as it would in an actual fire situation. The third test evaluated the ability of the prototype system to make multiple, real-time, line-of-sight optical thickness measurements in order to determine the location of a smoke plume.

3.3.1 Sensor Visibility and Smoke Detection

The ability of the video data gathering system to determine the activation of a temperature-sensitive, color-changing sensor was evaluated under a range of lighting conditions and smoke densities. To perform the evaluation a square array of nine sensors, spaced one meter apart, was suspended from the ceiling of a test enclosure. The sensors were numbered sequentially, left-to-right, in each row, beginning in the front row, as seen in

Fig. 10. The enclosure was 2.75 m deep, by 2.75 m wide, and 1.5 m high, with a ceiling constructed of 2.54 cm thick closed-cell polystyrene insulation. For test runs involving smoke, a back wall and two side walls constructed of heavy black plastic, and a clear acrylic front wall were installed. An exhaust fan was run to reduce the pressure in the test enclosure slightly below atmospheric,to prevent the escape of smoke from the enclosure. During all runs without smoke, the back, side and front walls and the exhaust fan were removed. The monitoring video camera was placed outside the test enclosure, at a distance of about four meters, so that all nine sensors were visible simultaneously.

The effect of lighting on sensor visibility was evaluated by varying the level of illumination on the sensors. Illumination in the enclosure was controlled by turning on from one to nine 60 Watt incandescent light bulbs placed around the floor of the enclosure. Light levels on the sensors in the enclosure were measured with a hand held photographic light meter. Visibility of the sensors was quantified by recording the average gray-scale pixel values of the digitized images of the sensors.

The effect of smoke on sensor visibility, and the ability of the video system to determine the optical density of smoke, were evaluated by measuring gray-scale pixel values of sensors obscured by known densities of smoke. The smoke, produced by a theatrical smoke machine, was allowed to uniformly fill the test enclosure. Once the enclosure was completely filled, the exhaust fan was turned on and the smoke was slowly evacuated from the enclosure. The average gray-scale pixel values of the black target, the white target, and the color-changing sheet in each sensor were recorded, as the smoke density decreased. At the same time, the optical density of the smoke in the enclosure was measured using light attenuation. The beam from a helium-neon laser was passed through the enclosure (3.66 m path length), and the intensity of the light which emerged was measured with a solid-state laser power meter. The optical density, D, of the smoke was taken to be

$$D = -10 \log_{10} (I/I_o) \qquad (10)$$

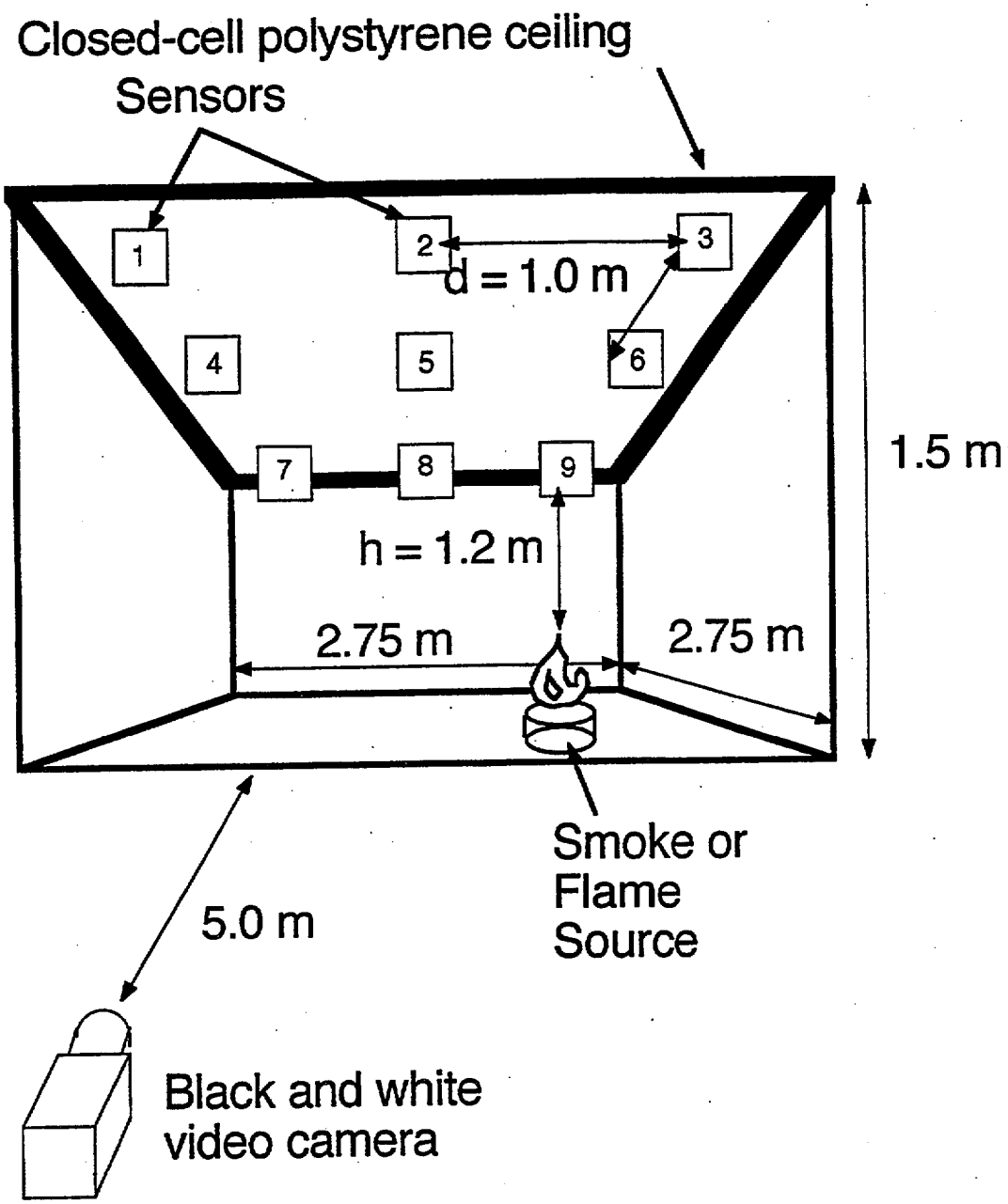

Figure 10. The test enclosure.

where D is in decibels, I is the intensity of the laser beam after passing through the smoke-filled enclosure, and I_o is the intensity of the laser beam after passing through a smoke-free enclosure.

3.3.2 Fire Location and Heat Release Rate Accuracy

The accuracy of the prototype fire detection system was evaluated by employing the fire detection system to detect a flame source placed in the test enclosure and determine the location and heat release rate of the flame source. The flame source used was a backpacker's camp stove which burned unleaded gasoline in a premixed flame. The height of the stove and its stand was approximately 0.30 m; giving a distance of 1.20 m from the stove flame to the enclosure ceiling. The thermal output of the camp stove was estimated to be Q_{act} = 2.4 kW, by measuring the mass flow of fuel in the stove (5.0×10^{-5} kg s^{-1}) and multiplying by the higher heating value of octane (4.8×10^{3} kJ kg^{-1}). Although this value of Q_{act} is clearly an over-estimate of thermal output, it is considered a suitable approximation for present purposes.

A test run was started by activating the prototype video fire detection system. Once running, the system monitored the status of all nine sensors in the test enclosure every 0.8 seconds. All test runs employed sensors with temperature-sensitive, color-changing sheets fabricated from microencapsulated TLC with an activation temperature of T_a = 32 C. The flame source (backpacker's camp stove) was ignited and then placed under the sensor array in the enclosure. As sensors were activated by the plume of hot gases rising from the flame source, the temperature-sensitive sheets changed color. As color changes were detected by the video system, the personal computer would record the location of the activated sensor and the sensor's time of activation. Once five sensors had been activated, and their color change detected, the personal computer would call the inverse problem solution algorithm. The algorithm would then take less than two seconds to determine the most probable location and heat release rate of the flame source.

The accuracy of the prototype video fire detection system was assessed in the same way the accuracy of the inverse problem solution algorithm was scored. Location error, ε_{loc},

was calculated by comparing the actual location of the camp stove flame source to the location determined by the prototype system:

$$\varepsilon_{loc} = \sqrt{\left(x_{pred} - x_{act}\right)^2 + \left(y_{pred} - y_{act}\right)^2} \qquad (10)$$

where (x_{act}, y_{act}) is the actual location of the camp stove and (x_{pred}, y_{pred}) is the prototype system's prediction of the location of the camp stove. The heat release rate error ratio, ε_Q, was taken to be the ratio of the heat release rate of the flame source predicted by the inverse problem solution algorithm, $Q_{pred}(t_{a,5})$, over the actual heat release rate of the flame source from which the data were taken, $Q_{act}(t_{a,5})$ (See Eq.(9)), where both heat release rates were determined for the time of the activation of the fifth sensor.

3.3.3 Smoke Plume Location

The ability of the video fire detection system to determine the location of a smoke plume was evaluated. Smoke plume location tests were made with the side walls and front window of the enclosure in place, but with the exhaust fan turned off. A test run began by activating the prototype fire detection system. The theatrical smoke machine was placed under the sensor array, at a set location on the floor in the enclosure. When the smoke machine was started up, it produced a well defined plume of smoke that rose to the ceiling and then turned, spreading out as a ceiling jet and filling the enclosure. As the smoke plume rose and filled the test enclosure, the average gray-scale pixel values of the digitized images of each of the nine sensors were recorded. Using the calibration curves for smoke density developed during the sensor visibility and smoke detection tests, the measured gray-scale pixel values for the black and white targets were converted into estimated optical thicknesses along each camera-to-sensor line of sight. Those line of sight optical thicknesses were then used to establish the location and density of the smoke plume.

3.4 Results: Prototype Fire Detection System Tests

3.4.1 Sensor Visibility and Smoke Detection

The effect of the level of illumination on sensor visibility is shown in Fig. 11. In that figure gray-scale pixel values of digitized sensor images taken by the prototype video fire detection system are plotted against the level of illumination on the sensors. Illumination is given in units of lux. Gray-scale pixel values are given as integer values from 0 to 255, since the frame-grabber is an eight-bit device. The value 0 represents the lowest level of brightness (black) while 255 represents the highest level of brightness (white). The figure shows average digitized gray-scale values for each of the black and white targets, and the temperature-sensitive, color-changing sheets (TLC and melt paint sheets), before and after activation. Recall that the black target was identical in appearance to the TLC temperature-sensitive, color-changing sheet before activation, and nearly identical to the melt paint sheet after activation.

Gray scale values for the black and white targets and the activated TLC sheets are all seen to increase as illumination levels rise from 75 lux to 210 lux. The increase is greatest for the black target and the activated TLC sheet at illumination levels less than 100 lux. At higher illumination levels the increase in gray-scale pixel values of the black target and activated TLC sheet are small. The gray-scale pixel values of the white target increases slowly at all levels of illumination.

Of more importance is the change in gray-scale values of the TLC sensor upon activation because it is this difference which must be detected to determine the TLC sensor activation. Figure 11 shows that the difference between gray-scale pixel values of unactivated TLC sheets (black target) and activated TLC sheets also grows as illumination increases. Below 90 lux the difference between activated and unactivated TLC sheets is extremely small, less than 10 or 4% of the full gray-scale range. Between 90 lux and 100 lux the difference in gray-scale pixel values of activated and unactivated TLC sheets rises sharply to 25 or 10% of the full gray-scale range. For levels of illumination above 100 lux, the difference in gray-scale values between activated and unactivated TLC sheets grows very

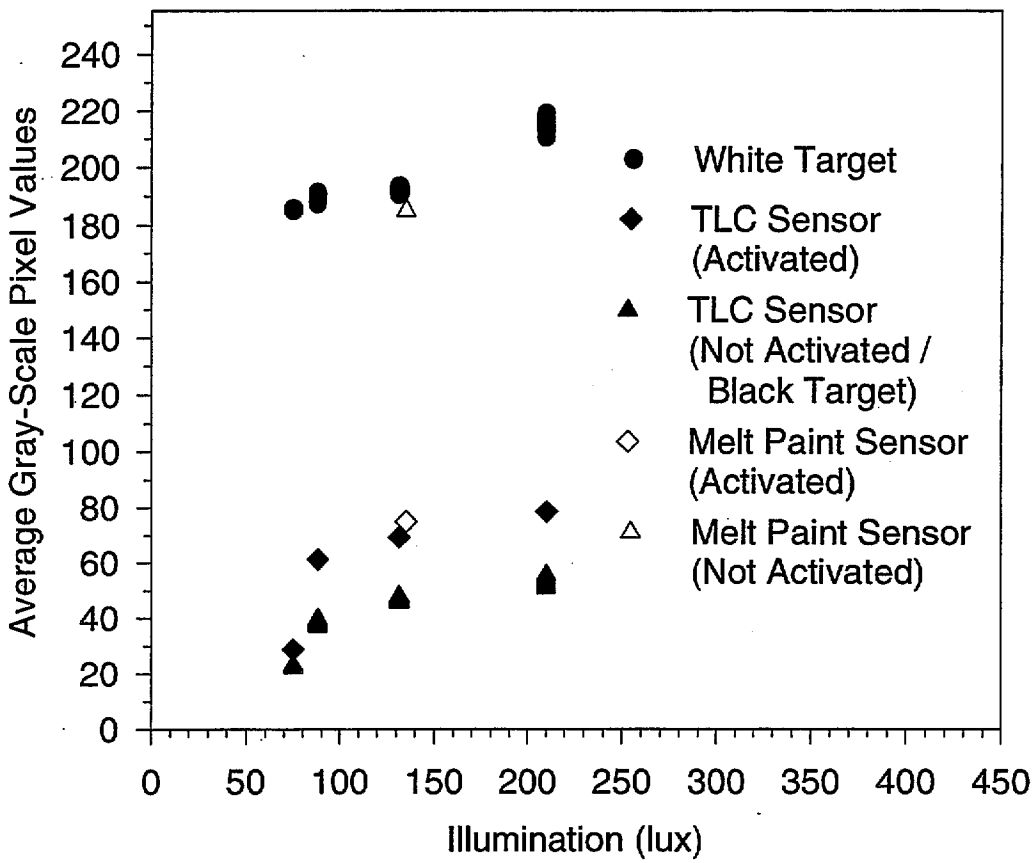

Fig. 11. Average gray-scale values of sensor images versus illumination.

slowly. In this plateau region, the detection of sensor activation will not be affected by changes in the level of illumination.

The small change in gray-scale pixel value upon activation, means that detecting the activation of TLC sheets is relatively difficult. Sensors based on melt-paint sheets display a greater change upon activation. Figure 11 shows the average gray-scale pixel values for a sensor with a melt-paint temperature-sensitive sheet, before and after activation. Only one level of illumination, 140 lux, is shown. Before activation, the melt-paint sheet is light in color, with an average gray-scale pixel value of 185. After activation the melt-paint becomes semi-transparent, revealing the black undercoat beneath. The activated melt-paint sensor has a gray-scale value of 75, close to the black target gray-scale value of 70 at the same illumination. The change in gray-scale value upon activation of the melt-paint sensor is quite large: 110 or more than 40% of the full gray-scale range. As a consequence, the use of this kind of temperature-sensitive, color-changing material produces a more robust sensor.

The effect of smoke on the visibility of the temperature-sensitive, color-changing TLC sheets is illustrated in Fig. 12. In the figure, the difference in gray-scale pixel values for a TLC sensor before and after activation are plotted against the optical density of smoke (in units of decibels) filling the test enclosure. The change in gray-scale values of the TLC sensor upon activation, is seen to decrease linearly from 25 or10% of full gray-scale range to a value of 15, or 6% of full range as smoke optical density increases from 0 to 7 db. To function under smoky conditions typical of a fire environment, the prototype video system must be capable of detecting changes of gray-scale values less than 15.

Figure 13 shows the effect of smoke on the visibility of the black and white targets in each sensor. In the figure, the difference between the average gray-scale pixel values of the black and white targets versus the optical density of smoke between the targets and the video camera is plotted. Data are shown for all nine sets of black and white targets. The difference in gray-scale pixel values of the black and white targets decreases linearly as smoke optical density increases, just as the difference in gray-scale values for the TLC sheets did. However, the difference between the black and white targets is much larger than that for the TLC sensors. The difference between black and white target gray scale values falls

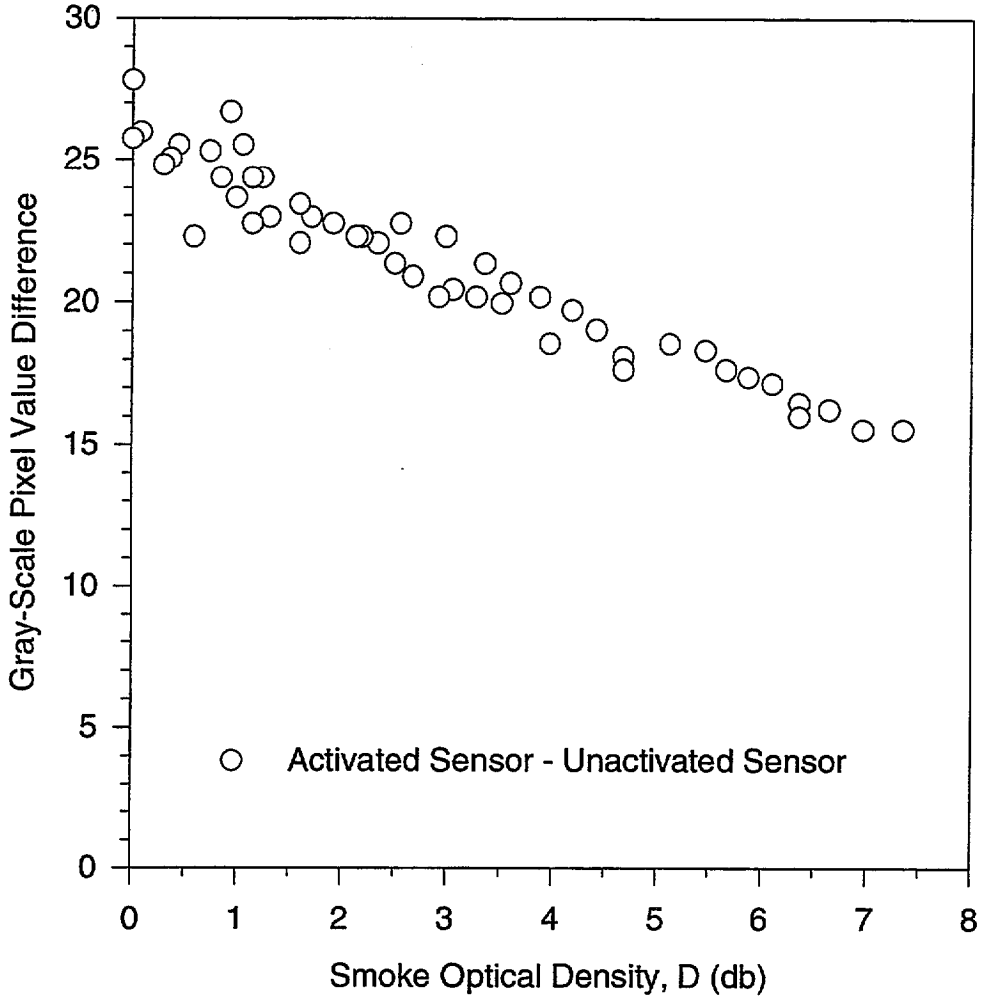

Fig. 12. Visibility of TLC sensor activation: difference between gray-scale pixel values of activated and unactivated sensors versus smoke optical density.

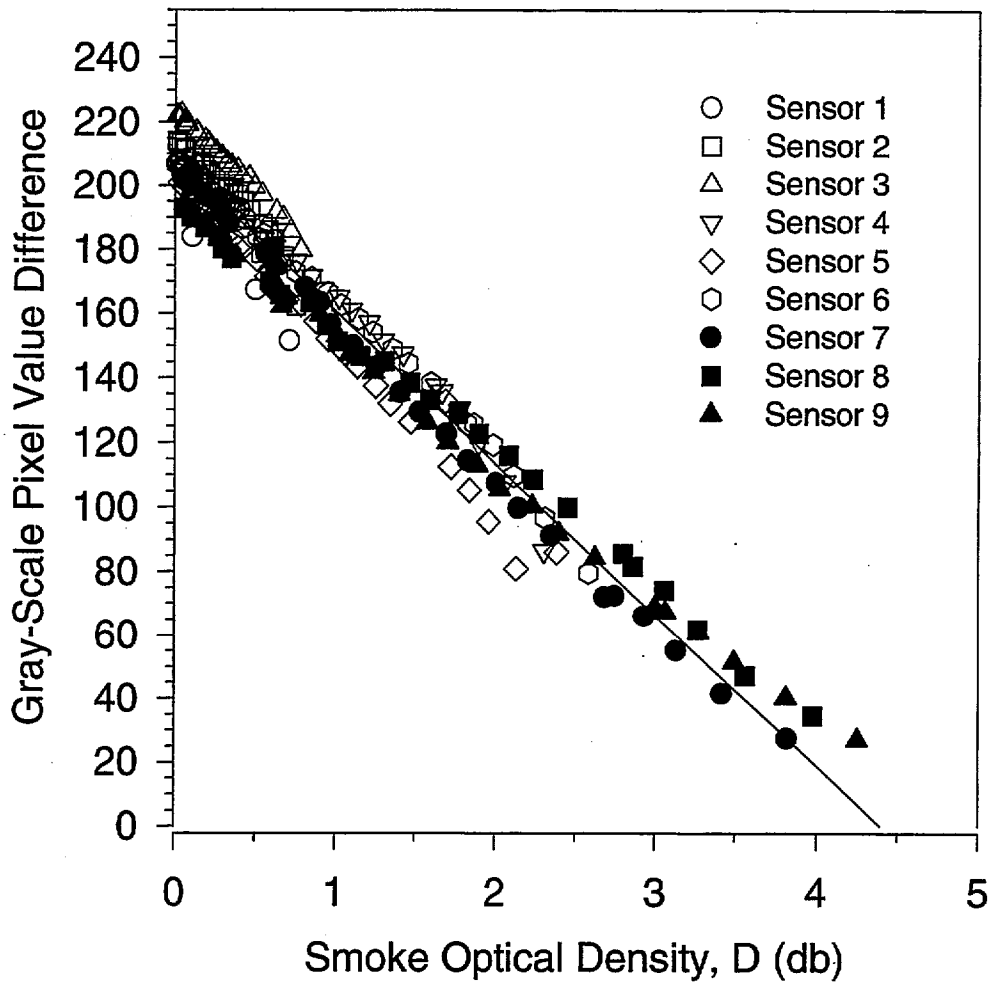

Fig. 13. Smoke obscuration of black and white targets: difference between gray-scale pixel values of black and white targets versus smoke optical density.

from a high of 210 (80% of full range) at 0 db to a low of 30 (10% of full range) at 4 db. The data for all nine sensors are seen to lie in a narrow band.

The large change in black and white target gray-scale values for the entire range of smoke optical densities seen in Fig. 13, means that the prototype fire detection system is able to detect small concentrations of smoke. The linear relationship between the black and white target gray-scale values and the smoke optical density, seen in Fig. 13, means that the prototype video fire detection system can be calibrated to make useful smoke optical density measurements along camera-to-sensor lines-of-sight.

3.4.2 Fire Location and Heat Release Rate Accuracy

The accuracy of the prototype video fire detection system in determining the location and heat release rate of a flame source can be judged by referring to Figs. 14 through 17. The figures show probability density functions (pdf's) for the prototype video fire detection system's location errors and heat release rate error ratios, as measured for experimental runs conducted in the test enclosure using 2.4 kW camp stoves as a flame sources.

Figure 14a gives the pdf for system location error and Fig. 14b gives the pdf for system heat release rate error ratio for 100 trials of the prototype system. All trials were conducted with the sensor spacing set at $d = 1.00$ m, the difference between sensor activation temperature and ambient temperature held constant at $\Delta T = 11$ C ($T_a = 33$ C, $T_{amb} = 22$ C) and the flame source heat release rate at $Q_{act} = 2.4$ kW.

The prototype video fire detection system is seen to have determined the location of the flame source in all 100 trials to within 0.50 m or to within one-half of the sensor spacing ($d/2$). The mean location error is much less, about 0.20 m, or $d/5$. Heat release rate error ratios for the 100 trials of the prototype system are seen to lie between the values of $\varepsilon_Q = 0.4$ and $\varepsilon_Q = 1.6$. In other words, the system was able to determine the heat release rate of the 2.4 kW flame source to within 60% in every test run. The mean heat release rate error ratio is $\varepsilon_Q = 1.1$, very close to a value of unity. The heat release rate error ratios for the

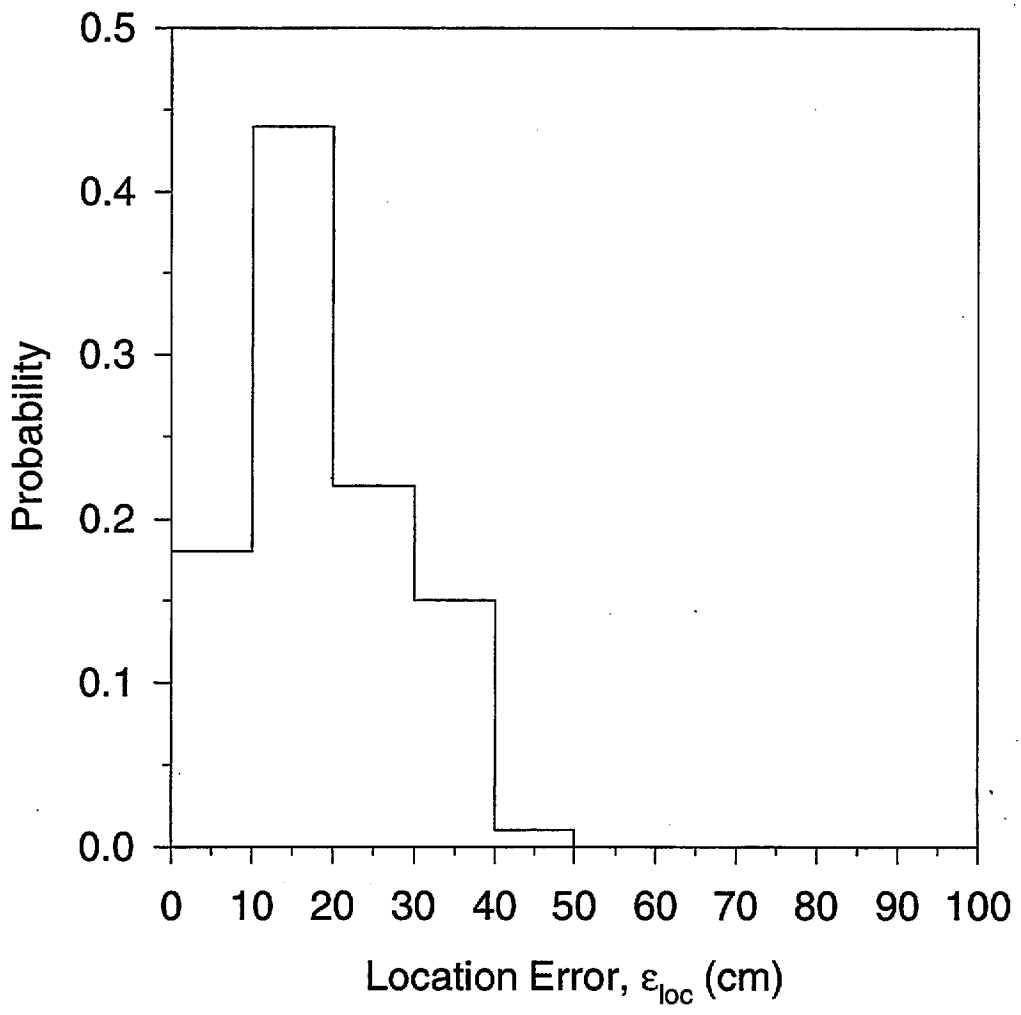

Fig. 14 a. Location error PDF for 100 trials at standard conditions: d = 1.00 m, ΔT = 1.1 C, Q_{act} = 2.4 kW.

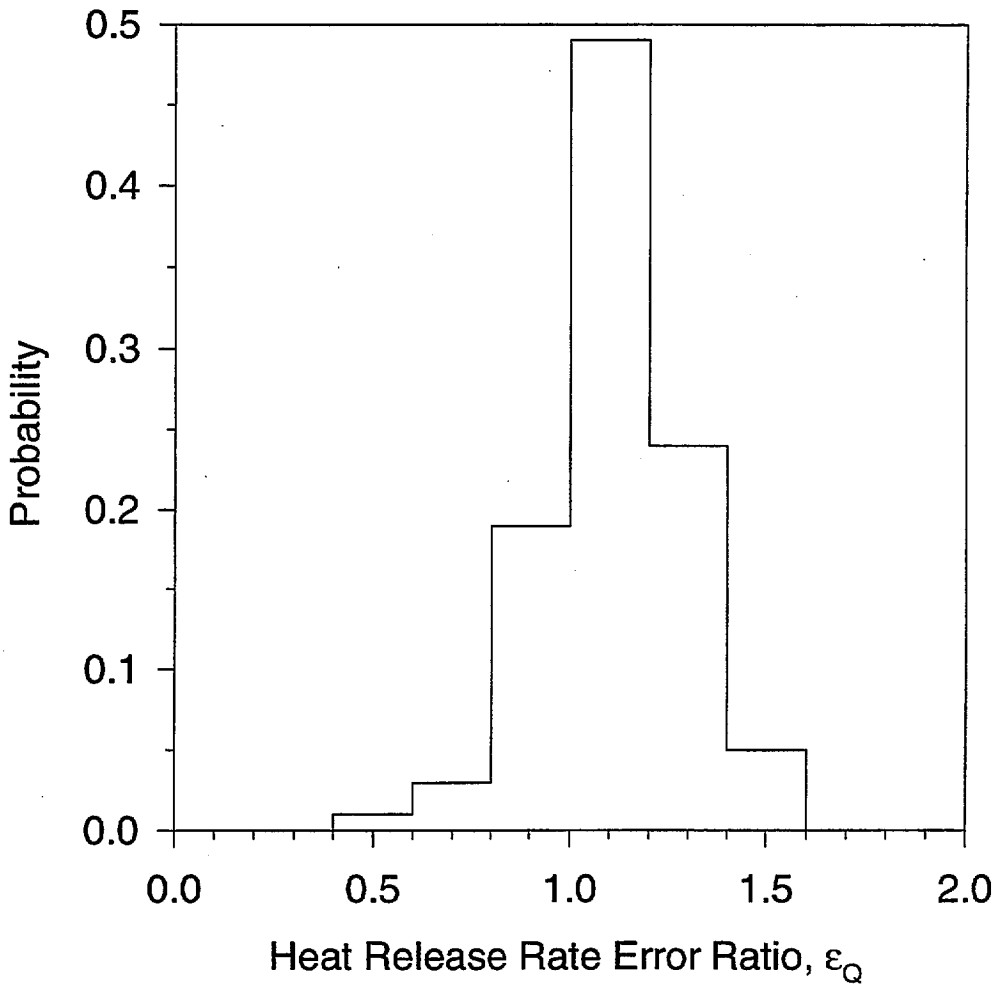

Fig. 14 b. Heat release rate error ratio PDF for 110 trials at standard conditions: d = 1.00 m, ΔT = 11 C, Q_{act} = 2.4 kW.

majority of the test runs lie in the range $\varepsilon_Q = 0.8$ to $\varepsilon_Q = 1.2$. In other words, the heat release rate of the flame source was predicted within 20% for most test runs.

Figures 15a and 15b demonstrate the effect of sensor spacing, d, on the accuracy of the prototype video system. Figure 15a gives the location error pdf and Fig. 15b gives the heat release rate error ratio pdf for 30 trials in which the sensor spacing was reduced to $d =$ 0.50 m. The difference between sensor activation temperature and ambient temperature was unchanged at $\Delta T = 11$ C ($T_a = 33$ C, $T_{amb} = 22$ C) and the flame source heat release rate was $Q_{act} = 2.4$ kW, as in the previous set of test runs.

The pdf's in Figs. 15a and b show that reducing the sensor spacing, d, causes errors in predictions of fire location to decrease while causing errors in predictions of fire heat release rate to increase. Location errors for all thirty runs are all less than $\varepsilon_{loc} = 0.30$ m, or just over $d/2$, while the mean location error is about $\varepsilon_{loc} = 0.15$ m or just under $d/3$. Heat release rate error ratios for the 30 trials range from $\varepsilon_Q = 0.2$ to $\varepsilon_Q = 0.6$, with a mean value of $\varepsilon_Q = 0.45$. In this case, with reduced sensor spacing, the prototype fire detection system underestimated the heat release rate of the flame source in all trials, and on average underestimated heat release rate by a factor of two.

The behavior seen in Figs. 15a and b can be understood in terms of the effect of sensor spacing, d, on random and systematic errors associated with measured sensor activation times. More specifically, the figures can be understood by looking at how the ratio of the magnitude of error in the sensor activation times to the magnitude of the sensor activation times themselves changes in each set of trials. The ratio is important because it is the ratio of error in activation time to activation time and not the absolute magnitude in the error which controls the accuracy of the inverse problem solution algorithm[4].

In Figs. 15a and b, reducing the sensor spacing, d, causes sensor activation times to be reduced. Reducing the sensor spacing does not affect the error associated with the measured sensor activation time. As a result, reducing sensor spacing causes the ratio of activation time error to activation time to increase. The increase in this ratio results in the increase in heat release rate errors seen in Fig. 15b. In contrast, the absolute location errors seen for the

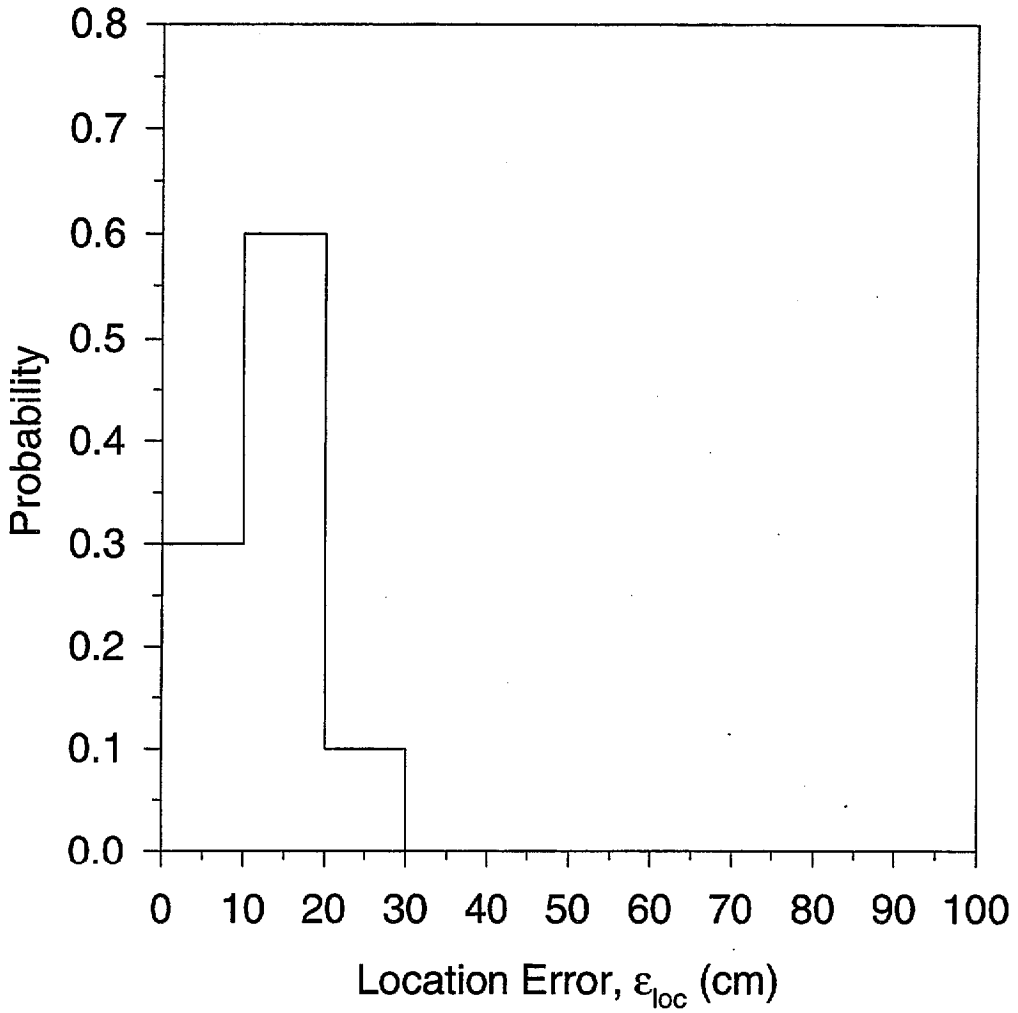

Fig. 15 a. Location error PDF for 30 trials at reduced sensor spacing: d = 0.50 m, ΔT = 11 C, Q_{act} = 2.4 kW.

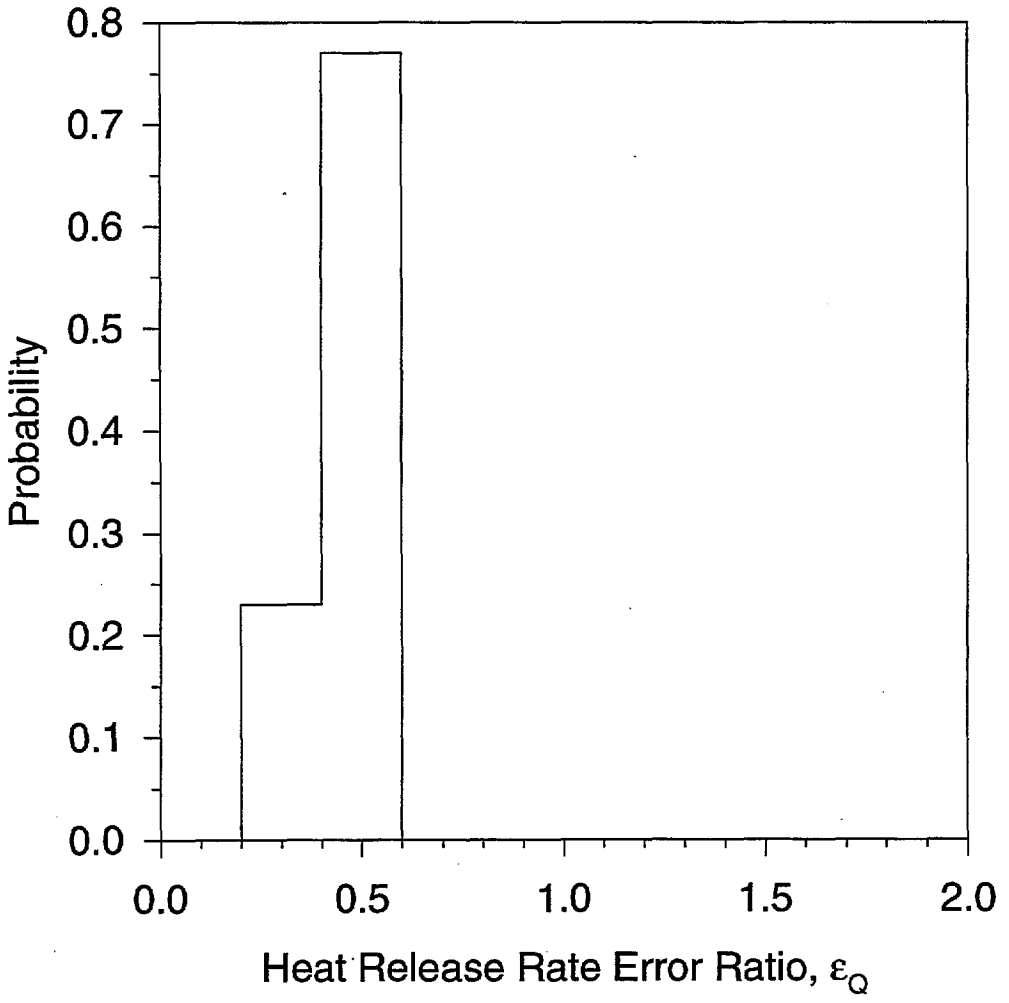

Fig. 15 b. Heat release rate error ratio PDF for 30 trials at reduced sensor spacing: d = 0.50 m, ΔT = 11 C, Q_{act} =2.4 kW.

reduced sensor spacing in Fig. 15a are smaller than those seen in Fig 14a. However, the location error normalized by sensor spacing increases as sensor spacing is reduced. Recall that in Fig. 14a, where d = 1.00 m, the mean location error is about d/5 while in Fig. 15a, where d = 0.50 m, the mean location error increases to d/3.

Figures 16a and 16b show the effect of the difference between sensor activation temperature and ambient temperature, $\Delta T = (T_a - T_{amb})$, on the accuracy of the prototype video system. Figure 16a gives the location error pdf and Fig. 16b gives the heat release rate error pdf for 30 trials in which the difference between activation and ambient temperatures has been reduced from ΔT = 11 C to ΔT = 6 C (T_a = 33 C, T_{amb} = 26 C). In all trials the sensor spacing spacing was d = 1.00 m, and the flame source heat release rate was Q_{act} = 2.4 kW.

The pdf's in Figs. 16a and b show that decreasing the temperature difference causes errors in predictions of both fire location and fire heat release rate to increase. In particular, for one-fifth of the trials (6 out of 30 trials), location errors are greater than ε_{loc} = 0.50 m, or more than $d/2$. The mean location error is ε_{loc} = 0.35 m or about $d/3$. The prototype system underpredicts the heat release rate of the flame source in all 30 trials. Heat release rate error ratios for the 30 trials lie in the range from ε_Q = 0.2 to ε_Q = 1.0, with a mean value of ε_Q = 0.55.

The behavior seen in Figs. 16a and b is similar to that seen in Figs. 15a and b. In Figs. 16a and b, reducing the difference between activation and ambient temperatures, ΔT, causes sensor activation times to be reduced, without affecting the error in activation time measurements, just as in Figs. 15a and b when sensor spacing, d, was reduced. Reducing ΔT, in the same way as reducing d, increases the ratio of activation time error to activation time. The result is an increase in both location error and heat release rate error for the prototype system. Note that the increases in location error and heat release rate error are similar in magnitude to those seen in Figs. 15a and b. In both cases the mean location error increases to $d/3$ and the mean heat release rate error ratio falls to about one-half.

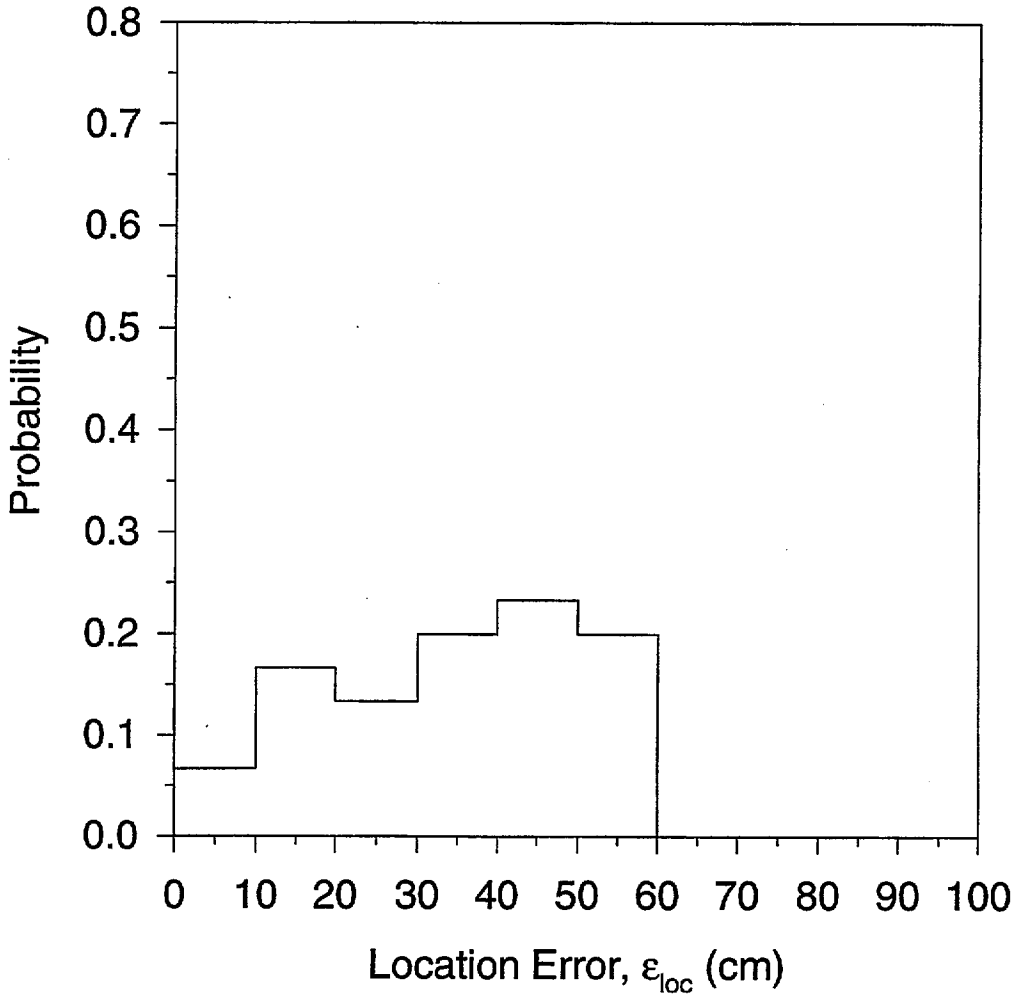

Fig. 16 a. Location error PDF for 30 trials at reduced difference between sensor activation temperature and ambient temperature: d = 1.00 m, ΔT = 6 C, Q_{act} = 2.4 kW.

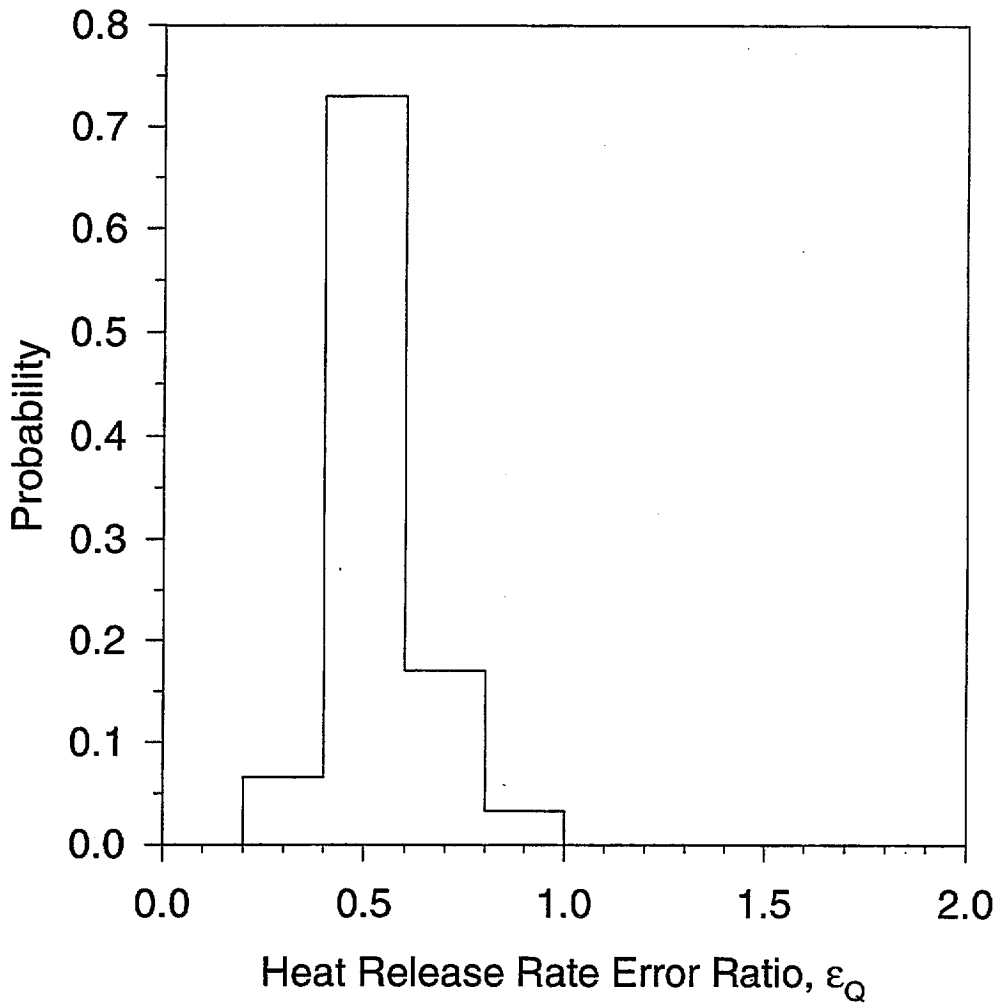

Fig. 16 b. Heat release rate error ratio PDF for 30 trials at reduced difference between sensor activation temperature and ambient temperature: D = 1.00 m, ΔT = 6 C, Q_{act} = 2.4 kW.

Figures 17a and 17b show the result of increasing the heat release rate of the flame source to Q_{act} = 4.8 kW, or double the value of Q_{act} = 2.4 kW used in earlier tests. The larger heat release rate was produced by placing two 2.4 kW camp stoves side by side in the test enclosure. Figure 17a gives the location error pdf and Fig. 17b gives the heat release rate error ratio pdf for 30 trials. The sensor spacing was d = 1.0 m, and the difference between sensor activation and ambient temperature was ΔT = 11 C.

The location error pdf in Fig. 17a is wider than for any previous case, ranging up to ε_{loc} = 0.70 m. The mean location error is ε_{loc} = 0.30 m or about $d/3$. Once again, the heat release rates determined by the prototype system are seen to be low, although not as low as in previous cases. Heat release rate error ratios range from ε_q = 0.4 to ε_q = 1.0. The mean heat release rate error ratio is ε_q = 0.7

The increases in location and heat release rate errors follow from the same reasons given for Figs. 15a and b, and 16a and b. In Figs. 17a and b, increasing the heat release rate of the flame source, Q_{act}, causes sensor activation times to be reduced, without affecting the error in activation time measurements, which increases the ratio of activation time error to activation time. In this case however, the increase in location error is larger than the increase in heat release rate error. The greater increase in location errors can be attributed in part, to the fact that two camp stoves, were used together to make up the flame source. These two camp stoves could not be placed closer to one another than about 0.20 m (center-to-center),and as a consequence the flame source was less like a point source than in previous cases.

3.4.3 Smoke Plume Location

The ability of the prototype video fire detection system to detect smoke and determine the optical density of the smoke has already been discussed. Recall that Fig. 13 showed that the difference between gray-scale pixel values of black and white targets could be correlated against the optical density of smoke along the line of sight between the sensor

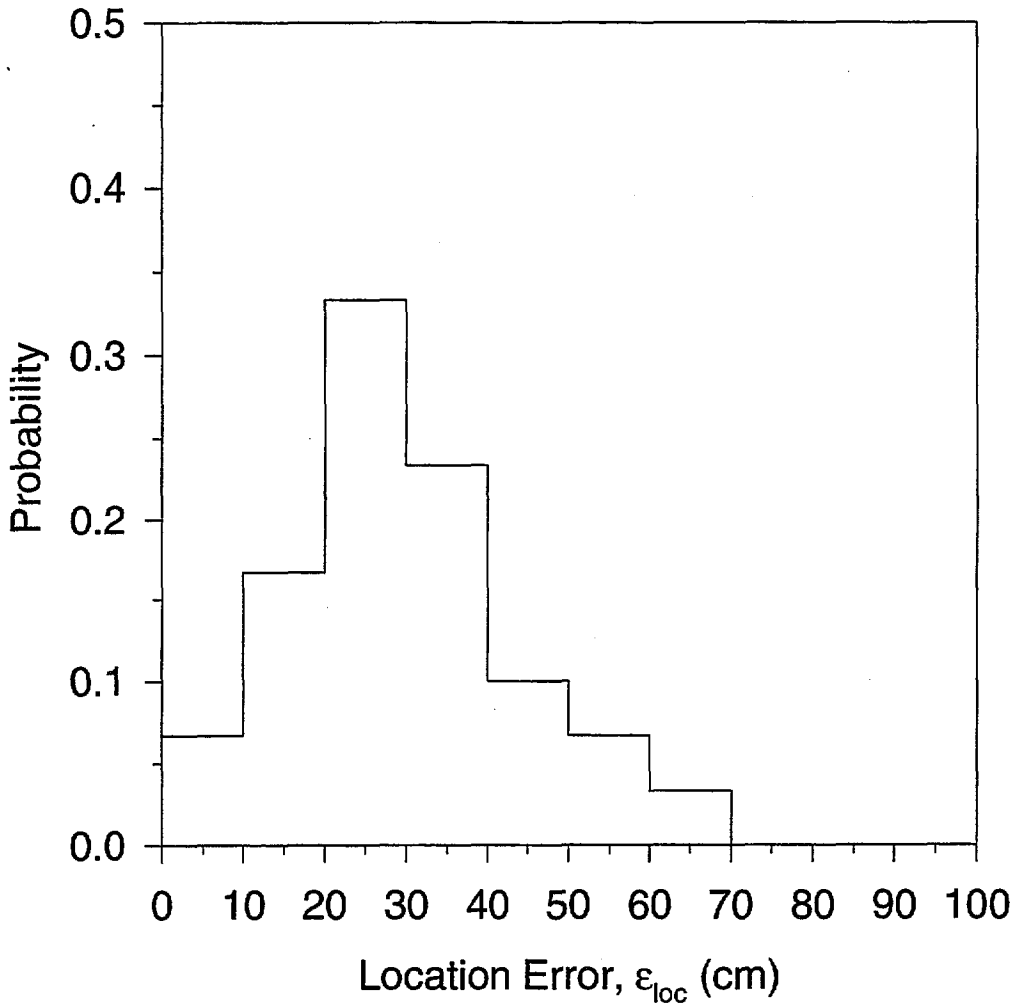

Fig. 17 a. Location error PDF for 30 trials at increased heat release rate: D = 1.00 m, ΔT = 11 C, Q_{act} = 4.8 kW.

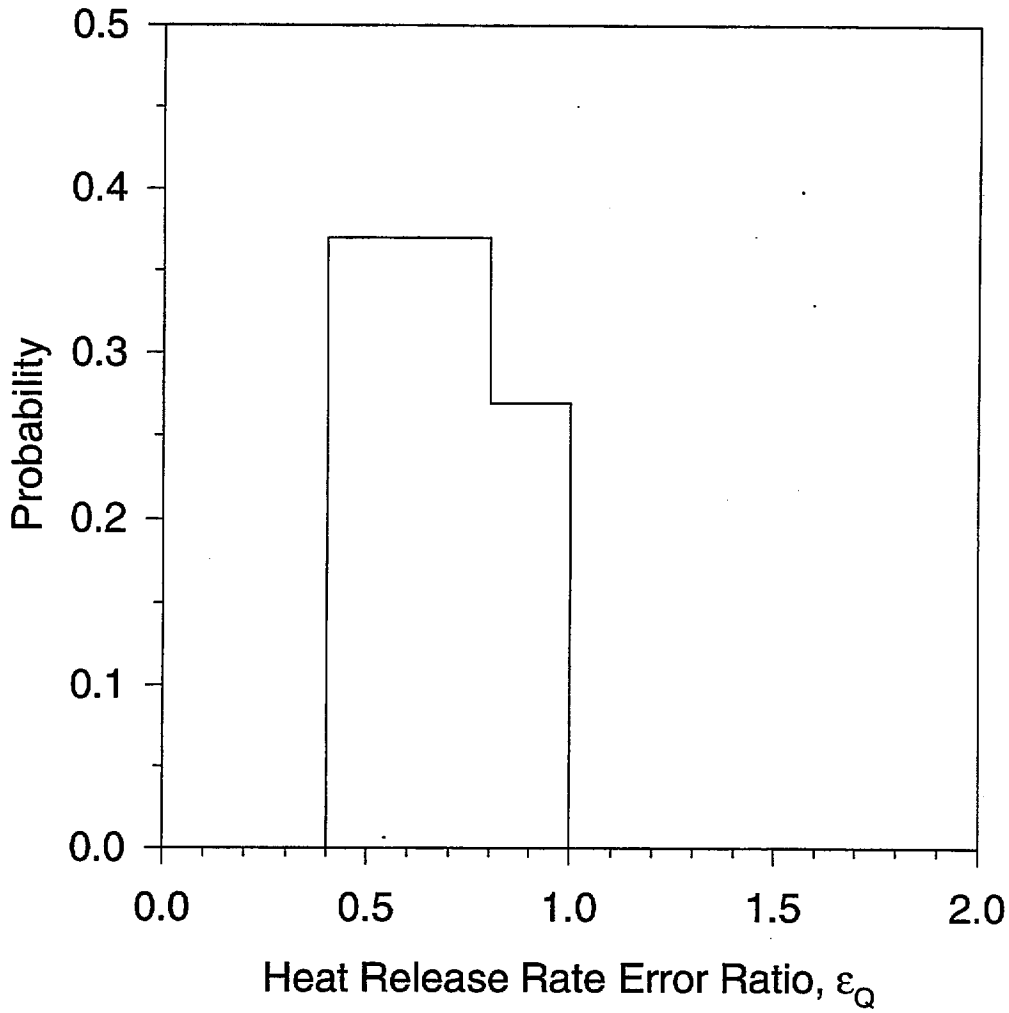

Fig. 17 b. Heat release rate error ratio PDF for 30 trials at increased heat release rate: d = 1.00 m, ΔT = 11 C, Q_{act} = 4.8 kW.

and the video camera. As a consequence, the availability of simultaneous line of sight optical density measurements from the camera to several sensors enables the system to track the location of a spreading smoke plume. Figure 18 shows how a smoke plume can be detected, located and tracked over time.

As described earlier, a smoke plume was created by a smoke generator placed in the enclosure. Figure 18 shows results when the smoke generator was placed below sensor four, located at the far left of the second row (position (2,3) in the figure). The figure represents line of sight optical density measurements for the nine sensors in the enclosure, at four elapsed times after the initiation of the smoke plume. Figure 18a shows the measurements after eight seconds had elapsed, Fig. 18b shows values after twelve seconds had elapsed, Fig. 18c after sixteen seconds had elapsed, and Fig. 18d after twenty seconds had elapsed. Before eight seconds no sign of the smoke can be detected. The arrival of the smoke plume at the ceiling of the enclosure is apparent after twelve seconds. Between sixteen and twenty seconds the smoke thickens in the vicinity of sensor four and the plume begins to spread obscuring sensors five and eight. Subsequent measurements showed the plume filling the entire ceiling of the enclosure.

4 Summary

A proposed method of detecting, locating and sizing an accidental fire, based on the solution of an inverse heat transfer problem, has been described. A working prototype video fire detection system which employs the inverse problem solution algorithm has been presented. The inverse heat transfer problem of interest is the convective heating of a compartment ceiling by the buoyant plume of combustion gases which rise from the fire. The inverse problem solution algorithm uses the fire model LAVENT as a forward model to predict the transient temperature field in a compartment given an assumed fire location and growth rate. The actual location and growth rate of the accidental fire is found by minimizing the sum of squares of the residuals of measured and predicted temperatures in the compartment. The prototype video fire detection system supplies the transient temperature data required by the inverse problem solution algorithm, through the

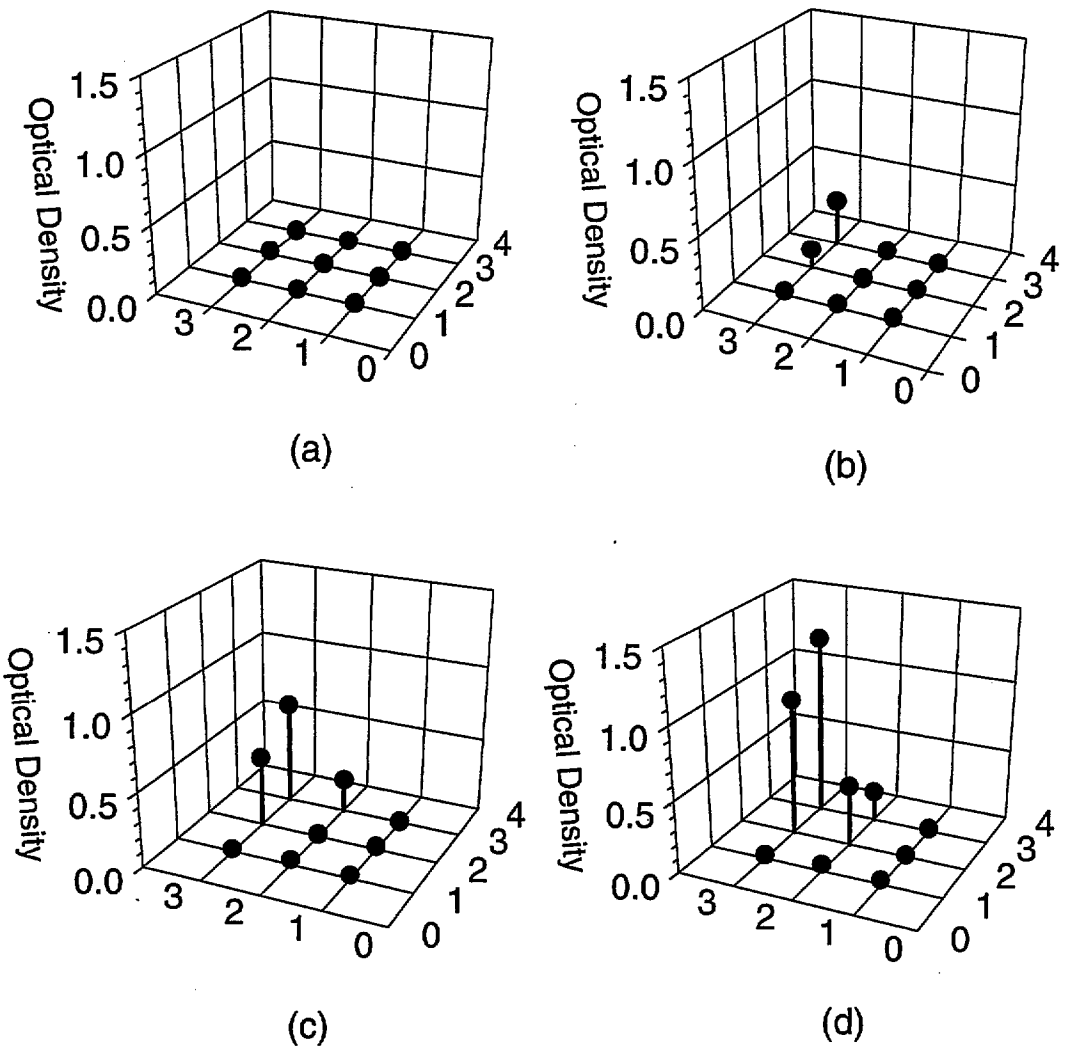

Fig. 18. Line of sight optical density measurements for all nine sensors in the test enclosure, during the growth of a smoke plume from a smoke generator placed under sensor four, at location (2,3). (a) t = 8 s, (b) t = 12 s, (c) t = 16 s, (d) t = 20 s.

use of a video camera which monitors temperature-sensitive, color-changing sensors distributed in an array on the ceiling of the compartment

A description and evaluation of the fire detection system has been presented in two parts. In the first part of the study, the theory behind the inverse problem method was presented and the development of the inverse problem solution algorithm was described. Two separate evaluations of the inverse problem solution algorithm were presented: (1) An evaluation based on the use of computer synthesized fire data, and (2) An evaluation based on data interpolated from measurements made in large-scale experimental burns.

In the first evaluation, sensor activation times were simulated and used as data for the inverse algorithm in order to delineate limits on the accuracy of the proposed fire detection system. The evaluation focused on the ability of the proposed fire detection system to locate and size accidental fires when systematic model errors in the forward problem solution and random measurement errors in the fire data were present. In particular it was shown that the accuracy of the inverse algorithm's location predictions was affected by the accuracy of the measurements of sensor activation times, but was not affected by the accuracy of the forward problem model. In contrast the accuracy of the inverse algorithm's heat release rate predictions was affected both by the accuracy of sensor activation time measurements and by the accuracy of the forward problem model. The effect of random errors in sensor activation time measurements was to widen the distribution of heat release rate error ratios. The effect of systematic errors in the forward problem solution was to shift the peak of the heat release rate error ratio distribution away from unity. The significant effect of model error on heat release rate predictions and conversely the lack of an effect of model error on location predictions made the task of determining the heat release rate of a fire more challenging and more subject to error than the task of locating a fire.

In the second evaluation, the inverse problem solution algorithm was tested using fire data interpolated from experimental measurements taken in a large-scale test burn. The results of the second evaluation were compared to the previous results for the inverse algorithm based on computer simulated fire data. Results of the two tests were shown to be

similar, when random and systematic errors of appropriate magnitude were applied to the simulated data. The comparison demonstrated the validity of the use of computer simulated data to determine limits on the performance of the inverse problem solution algorithm, as long as the simulated data incorporated realistic levels of error.

The evaluation of the inverse problem solution algorithm using interpolated fire data also indicated the level of accuracy that could be expected of the proposed fire detection system operating in a large scale industrial environment. The inverse problem solution algorithm was able to locate most fires within one-third of the distance between sensors and 95% of all fires within two-thirds of the distance between sensors. The algorithm was able to determine the heat release rate of most fires to within a factor of three, and the heat release rate of 95% of all fires to within a factor of five.

The second part of the study focused on the operation of a working prototype video fire detection system and its performance under laboratory conditions. The prototype fire detection system, employed a video camera to monitor an array of temperature-sensitive, color-changing sensors, and an inverse problem solution algorithm to determine the location and heat release rate of an accidental fire. The operation of the prototype fire detection system has been described in terms of its two major components: the video data-gathering hardware and the inverse problem solution software.

The video data-gathering hardware consisted of the array of sensors, the video camera which monitored them, and a frame grabber which digitized the video images and passed them on to a personal computer. Data gathered by the prototype system included transient temperature information, and line of sight smoke optical thickness information.

The inverse problem solution software consisted of a personal computer based FORTRAN algorithm. The algorithm used the times of activation of five ceiling mounted temperature sensors gathered by the video hardware as data. The inverse algorithm determined the most probable location and heat release rate of the fire, by comparing the activation times for the five sensors to the activation times predicted by the zone fire model LAVENT.

Two candidate (commercially available) temperature-sensitive, color-changing materials were evaluated as possible sensor materials: a thermochromic liquid crystal (TLC) paint, and a temperature-indicating melt paint. The color change of sensors fabricated with the TLC paint was shown to be detectable by the video camera used in the present study, at illumination levels as low as 100 lux and through smoke with optical density as great as 7 db. However, the change in gray-scale value of the TLC sensors upon activation was small. In contrast the change in gray-scale value of sensors fabricated from the melt paint was much greater. As a consequence, sensors fabricated with the temperature-indicating melt paint would be significantly easier to monitor than the TLC sensors.

The prototype video fire detection system's accuracy in determining the location and heat release rate of a flame source was evaluated. The evaluation consisted placing a 2.4 kW backpacker's camp stove in a 2.75 m x 2.75 m x 1.75 m model enclosure monitored by the video detection system. In a set of 100 trials, the prototype system located the camp stove flame source to within one-half the sensor-to-sensor spacing, $d/2$, in all trials and located the flame source to within one-fifth of the sensor-to-sensor spacing, $d/5$, in most of the trials. In the same set of 100 trials, the prototype system determined the heat release rate of the flame source to within a factor of three in all trials, and determined the heat release rate of the flame source to within 20% in most of the trials.

The accuracy of the inverse problem solution algorithm depended on the ratio of the magnitude of errors in measured sensor activation times to the magnitude of the activation times. Increasing this ratio by reducing the sensor spacing, d, reducing the difference between ambient and sensor activation temperatures, ΔT, or increasing the flame source's heat release rate, Q_{act}, caused increases in both location and heat release rate errors. However, for the entire range of variables tested, the prototype system was able to determine the location of the flame source to within one half the sensor-to-sensor spacing, $d/2$ for most test runs. The prototype system was able to determine the heat release rate of the flame source to within a factor of five for all test runs.

The ability of the prototype video system to make approximate optical thickness measurements along camera to sensor lines of sight was demonstrated. Gray-scale pixel

value measurements from video images of black and white targets on the array of sensors were calibrated against optical thickness as measured by laser light attenuation. The ability of the system to use these line of sight optical thickness measurements to locate a smoke plume, and track its growth was demonstrated.

Nomenclature

a	Systematic error parameter: constant bias (s)
b	Systematic error parameter: constant fraction
c_1, c_2, c_3, c_4	Correlation constants: eq. 8
D	Optical depth from Eq. 1
d	Distance between sensors (m)
$G(\sigma)$	Gaussian distribution of random measurement error with standard deviation
σ	
h	Height of ceiling (m)
I	Intensity of laser beam passing through smoke-filled enclosure ($Wm^{-2}St^{-1}$)
I_o	Intensity of laser beam passing through smoke-free enclosure ($Wm^{-2}St^{-1}$)
n	Number of sensors
Q	Fire heat release rate (W)
Q_{act}	Fire heat release rate reported for large-scale burns in Ref 8, or
	Actual fire heat release rate for flame source (W)
Q_{sim}	Simulated fire heat release rate (W)
Q_{pred}	Fire heat release rate predicted by inverse problem solution algorithm, or
	Flame source heat release rate predicted by prototype detection system (W)
S	Sum of squares: eq. 4
T	Temperature (K)
T_{amb}	Ambient temperature (K)
T_a	Sensor activation temperature (K)
t_i	Predicted activation time of i^{th} sensor (s)
$t_{a,i}$	Predicted elapsed time between activation of i^{th} and 1^{st} sensors (s)
t_i	Measured activation time of i^{th} sensor (s)
$t_{a,i}$	Measured elapsed time between activation of i^{th} and first sensors (s)
$t_{LAV,i}$	LAVENT simulated elapsed time between activation of i^{th} and 1^{st} sensors (s)
r	Radial distance from fire (m)
(x,y)	Fire location (m)

(x_{act}, y_{act})	Actual flame source location (m)
(x_{sim}, y_{sim})	Simulated fire location (m)
(x_{pred}, y_{pred})	Fire location predicted by inverse problem solution algorithm, or Flame source location predicted by prototype fire detection system (m)

Greek letters

α	Fire growth rate (Ws^{-2})
α_{sim}	Simulated fire growth rate (Ws^{-2})
α_{pred}	Fire growth rate predicted by inverse problem solution algorithm (Ws^{-2})
ε_{loc}	Location error (m)
ε_Q	Heat release rate error ratio
σ	Standard deviation of normally distributed random measurement error
ΔT	$(T_a - T_{amb})$

References

1. Nelson, D.F., *Annual Conf. on Fire Research: Book of Abstracts*, National Institute of Standards and Technology, Gaithersburg, MD. (1993).
2. Milke, J.A., Hagen, B.C., McAvoy, T.J., and Pan, D., *NISTIR 5499*, National Institute of Standards and Technology, Gaithersburg, MD. (1994).
3. Falco, L. and Debergh, P., *Proceedings of AUBE '89*, University of Duisburg, Germany, (1989).
4. Jarny, Y., Ozisik, M.N., and Bardon, J.P., *Int. J. Heat Mass Transfer*, 34,(1991) 2911.
5. Padakannaya, K., Richards, R.F., and Plumb, O.A., in Bryan, W.J., and Beck, J.V. (ed.), *Proceedings of the 30th National Heat Transfer Conference*, HTD-Vol. 312, (1995), 63.
6. Moutsoglu, A., *Journal of Heat Transfer*, 111, (1989) 37.
7. Heskestad, G., *Society of Fire Protection Engineers*, Technology report 82-8 (1982).
8. Cooper, L.Y., *Fire Safety Journal*, 16, (1990) 137.
9. Heskestad, G., and Delichatsios, M.A., *17th Symposium (International) on Combustion*, (1985) 1113.

NIST-114
(REV. 6-93)
ADMAN 4.09

U.S. DEPARTMENT OF COMMERCE
NATIONAL INSTITUTE OF STANDARDS AND TECHNOLOGY

MANUSCRIPT REVIEW AND APPROVAL

(ERB USE ONLY)
ERB CONTROL NUMBER | DIVISION
PUBLICATION REPORT NUMBER: NIST-GCR-96-695 | CATEGORY CODE
PUBLICATION DATE: July 1996 | NUMBER PRINTED PAGES

INSTRUCTIONS: ATTACH ORIGINAL OF THIS FORM TO ONE (1) COPY OF MANUSCRIPT AND SEND TO THE SECRETARY, APPROPRIATE EDITORIAL REVIEW BOARD

TITLE AND SUBTITLE (CITE IN FULL)

DEVELOPMENT OF AN ECONOMICAL VIDEO BASED FIRE DETECTION AND LOCATION SYSTEM

CONTRACT OR GRANT NUMBER: 60NANB2D1290

TYPE OF REPORT AND/OR PERIOD COVERED:

AUTHOR(S) (LAST NAME, FIRST INITIAL, SECOND INITIAL)
Plumb, O.A., and Richards, R.F.
Department of Mechanical and Materials Engineering
Washington State University, Pullman, WA 99164-2920

PERFORMING ORGANIZATION (CHECK (X) ONE BOX)
[ ] NIST/GAITHERSBURG
[ ] NIST/BOULDER
[ ] JILA/BOULDER

LABORATORY AND DIVISION NAMES (FIRST NIST AUTHOR ONLY)

SPONSORING ORGANIZATION NAME AND COMPLETE ADDRESS (STREET, CITY, STATE, ZIP)
U.S. Department of Commerce
National Institute of Standards and Technology, Gaithersburg, MD 20899

PROPOSED FOR NIST PUBLICATION

[ ] JOURNAL OF RESEARCH (NIST JRES)	[ ] MONOGRAPH (NIST MN)	[ ] LETTER CIRCULAR
[ ] J. PHYS. & CHEM. REF. DATA (JPCRD)	[ ] NATL. STD. REF. DATA SERIES (NIST NSRDS)	[ ] BUILDING SCIENCE SERIES
[ ] HANDBOOK (NIST HB)	[ ] FEDERAL INF. PROCESS. STDS. (NIST FIPS)	[ ] PRODUCT STANDARDS
[ ] SPECIAL PUBLICATION (NIST SP)	[ ] LIST OF PUBLICATIONS (NIST LP)	[X] OTHER NIST-GCR
[ ] TECHNICAL NOTE (NIST TN)	[ ] NIST INTERAGENCY/INTERNAL REPORT (NISTIR)	

PROPOSED FOR NON-NIST PUBLICATION (CITE FULLY) [ ] U.S. [ ] FOREIGN

PUBLISHING MEDIUM
[X] PAPER [ ] CD-ROM
[ ] DISKETTE (SPECIFY)
[ ] OTHER (SPECIFY)

SUPPLEMENTARY NOTES

ABSTRACT (A 2000-CHARACTER OR LESS FACTUAL SUMMARY OF MOST SIGNIFICANT INFORMATION. IF DOCUMENT INCLUDES A SIGNIFICANT BIBLIOGRAPHY OR LITERATURE SURVEY, CITE IT HERE. SPELL OUT ACRONYMS ON FIRST REFERENCE.) (CONTINUE ON SEPARATE PAGE, IF NECESSARY.)

A method of detecting, locating, and sizing accidental fires based on the solution of an inverse heat transfer problem is described and a prototype video fire detection system employing that method is presented. The inverse heat transfer problem to be solved is that of the convective heating of a compartment ceiling by the hot plume of combustion gases rising from an accidental fire. An inverse problem solution algorithm capable of determining the location and heat release rate of the fire employing transient temperatures at the ceiling of the compartment as data is developed. A prototype system based on the use of a video camera to monitor an array of temperature-sensitive, color-changing sensors and capable of supplying the transient temperature data needed by the inverse problem solution algorithm is described. The limits on the accuracy of the inverse problem solution algorithm are demonstrated by exercising the algorithm, on transient temperature data from computer simulated compartment fires. The performance of the prototype video fire detection system is demonstrated by employing it to determine the location and heat release rate of a small flame source in a lab scale test enclosure.

KEY WORDS (MAXIMUM OF 9; 28 CHARACTERS AND SPACES EACH; SEPARATE WITH SEMICOLONS; ALPHABETIC ORDER; CAPITALIZE ONLY PROPER NAMES)
caneras; fire detection systems; fire protection; fire research; heat transfer; industrial plants

AVAILABILITY
[X] UNLIMITED [ ] FOR OFFICIAL DISTRIBUTION - DO NOT RELEASE TO NTIS
[ ] ORDER FROM SUPERINTENDENT OF DOCUMENTS, U.S. GPO, WASHINGTON, DC 20402
[X] ORDER FROM NTIS, SPRINGFIELD, VA 22161

NOTE TO AUTHOR(S): IF YOU DO NOT WISH THIS MANUSCRIPT ANNOUNCED BEFORE PUBLICATION, PLEASE CHECK HERE. [ ]

WORDPERFECT